



T.C.

ALTINBAS UNIVERSITY

Electrical and Computer Engineering

**EVALUATION OF WATER STATE USING  
COMBINED TEMPORAL REMOTE SENSING  
AND IMAGE PROCESSING TECHNIQUES**

Faten Azeez Alani

Supervisor: Prof. Dr. Oguz BAYAT

Istanbul, (2019)

**EVALUATION OF WATER STATE USING COMBINED TEMPORAL  
REMOTE SENSING AND IMAGE PROCESSING TECHNIQUES**

by

**Faten Azeez Alani**

Electrical and Computer Engineering

Submitted to the Graduate School of Science and Engineering

in partial fulfillment of the requirements for the degree of

Doctor of Philosophy

ALTINBAŞ UNIVERSITY

2019

This is to certify that we have read this thesis and that in our opinion it is fully adequate, in scope and quality, as a thesis for the degree of Doctor of Philosophy.

---

Prof. Dr. Oğuz BAYAT

Supervisor

Examining Committee Members (first name belongs to the chairperson of the jury and the second name belongs to supervisor)

Prof. Dr. Oğuz BAYAT	School of Engineering and Natural Science, Altinbas University	_____
Asst. Prof. Dr. Çağatay AYDIN	School of Engineering and Natural Science, Altinbas University	_____
Asst. Prof. Dr. Çağdas ATILLA	School of Engineering and Natural Science, Altinbas University	_____
Asst. Prof. Dr. Adil Deniz DURU	Faculty of Sport Science, Marmara University	_____
Prof. Dr. Hasan Hüseyin BALIK	Air Force Academy, National Defense University	_____

I certify that this thesis satisfies all the requirements as a thesis for the degree of Doctor of Philosophy.

---

Asst. Prof. Çağatay AYDIN

Head of Department

Approval Date of Graduate School of  
Science and Engineering: \_\_\_\_/\_\_\_\_/\_\_\_\_

---

Prof. Dr. Oğuz BAYAT

Director

I hereby declare that all information in this document has been obtained and presented in accordance with academic rules and ethical conduct. I also declare that, as required by these rules and conduct, I have fully cited and referenced all material and results that are not original to this work.

Faten Azeez Alani

## **DEDICATION**

To the spirit of my parents, with pride.



## **ACKNOWLEDGEMENTS**

Firstly, I would like to thank deeply the God who gave me patience and strength to complete this work, praise and appreciate to him.

Then, I would like to express my sincere thanks and gratitude to my advisor Prof. Dr. Oguz Bayat, for his continues support, guidance through all steps of the work, for his patience, motivation and immense knowledge. His supervision encourages and helps me how to be responsible by myself in all the period of working on research and writing this thesis, I hope all the best for him in all areas of life.

Besides, I would like to thanks the rest of my thesis committee for their insightful comments and cooperation.

My sincere thank as well should goes to the Ministry of Higher Education in Iraq for provided me an opportunity to get scholarship for PhD studying. And I greatly appreciate the staff at Mosul University for their assistance.

I am very indebted to all Remote Sensing Center staff instructors and professors for their advices to grow up the research, without their precious support it would not be possible to conduct this research.

Thanks to all my family and friends who encouraged and supported me in all parts of my life for furthering education.

Last, but not least, my deep thank goes to my colleagues during PhD study and classmates for supporting me spiritually throughout working in research and writing this thesis.

## **ABSTRACT**

# **EVALUATION OF WATER STATE USING COMBINED TEMPORAL REMOTE SENSING AND IMAGE PROCESSING TECHNIQUES**

Alani, Faten Azeez

PhD, Electrical and Computer Engineering, Altınbaş University,

Supervisor: Prof. Dr. Oguz BAYAT

Date: Jun, 2019

Pages: 91

Remote sensing (RS) has significant role for detecting and monitoring different objects on the earth through the analysis of data which acquired by various types of sensors. Monitoring capacity and level of water resources is an important matter for different fields. This work demonstrated the efficiency of MATLAB software to monitor the water state in Mosul Dam Reservoir which is located in the North West of Mosul city over the period of years between (1986-2017). In this work, various digital image processing (DIP) algorithms were performed and Multi Spectral (MS) temporal Landsat data were acquired over time period. Two main steps were processed, preprocessing which illustrated how to prepare the Landsat's data to be more accurate for extracting the information, and post processing step implement various digital image processing techniques that included integration and hybridization between two processing methods in the stage that led to gain the target of this work with high performance. Different objective functions criteria's were performed to test the performance and the accuracy of the proposed work, regarded to the adopted method. In other word, Peak Signal To Noise Ratio

(PSNR) and Mean Square Error (MSE) were utilized for the obtaining the performance of coastline detection as a first stage. Furthermore, the Assessment Accuracy (AC) depending on different values had demonstrated the performance of hybrid classification method for classification the quality of Water Lake. Consequently, it is infer that this work gave a futuristic view for the status of water state monitoring through combined applications related to temporal data and image processing. As well as, its concentrated on the evaluation of water state areas in Mosul city and Mosul Dam Lake due to its importance for providing the electricity to the Mosul city. It is also considered one of the most important tourist lakes in Iraq. So the attention about this area is significant for most researchers who interested on water resources studying.

**Keywords:** Temporal Remote Sensing Data, Water monitoring, Image processing, combined processing, Hybrid classification, MATLAB.



# TABLE OF CONTENTS

	<u>Pages</u>
<b>LIST OF TABLES .....</b>	<b>xii</b>
<b>LIST OF FIGURES .....</b>	<b>xiii</b>
<b>LIST OF ABBREVIATIONS .....</b>	<b>xv</b>
<b>1. INTRODUCTION .....</b>	<b>17</b>
1.1 DESCRIPTION OF STUDY AREA.....	17
1.2 MATERIAL AND DATA SET.....	18
1.3 DESCRIPTION OF DATA SET.....	18
1.4 MAIN OUTLINES .....	20
1.5 OBJECTIVE AND ACHIVMENT OF WORK.....	21
<b>2. BACKGROUND.....</b>	<b>22</b>
2.1 BASIC OF REMOTE SENSING .....	22
2.1.1 Remote Sensing in Water Resources.....	23
2.1.2 Representing Landsat Satellite Data.....	24
2.2 SPECTRAL RESOLUTION .....	25
2.3 SPATIAL RESOLUTION.....	25
2.4 LITERTURE RIVEW .....	26
2.4.1 Normalization Difference Water Index Method (NDWI) .....	26
2.4.2 Wavelet Transform (WT).....	27
2.4.2.1 Discrete wavelet transform (DWT) .....	27
.....	28
2.4.3 Morphological Techniques .....	28
2.4.4 Classification .....	28
2.4.4.1 K-Means clustering.....	28
2.4.4.2 Support vector machine (SVM).....	29
<b>3. WATER SURFACE EXTRACTION VIA IMAGE PROCESSING TECHNIQUES</b>	<b>30</b>

3.1	METHODOLOGY FOR WATER EXTRACTION .....	30
3.2	IMAGE PREPROCESSING .....	30
3.2.1	Input Data Set .....	31
3.2.2	Geometric Correction .....	31
3.2.3	Bands Combination .....	32
3.2.4	Crop Region of Study Area (ROA) .....	33
3.2.5	Contrast Enhancement .....	33
3.3	WATER SURFACE EXTRACTION (WSE) .....	33
3.3.1	Reservoir Coastline Extraction .....	34
3.3.1.1	Normalized difference water extraction (NDWI) .....	35
3.3.1.2	Wavelet transform (WT) .....	36
3.3.1.3	Gabor wavelet transform (GWT) .....	37
3.3.2	Mathematical Morphological Operations (MMO) .....	38
3.4	PERFORMANCE CRETERIA (AC) .....	39
<b>4.</b>	<b>EVALUATION OF WATER STATE .....</b>	<b>43</b>
4.1	MONITORING WATER LEVEL (MWL) .....	43
4.1.1	Reservoir Area Extraction (RAE) .....	44
4.2	MONITORING WATER QUALITY (MWQ) .....	45
4.2.1	Hybrid Classification .....	46
4.3	PERFORMANCE ACCURACY (AC) .....	48
<b>5.</b>	<b>FEATURES EXTRACTION.....</b>	<b>55</b>
5.1	LAND USE LAND COVER CLASSIFICATION (LULCC) .....	55
5.2	HYBRID APPROACH .....	56
5.3	PROPOSED LAND COVER CLASSIFICATION ALGORITHMS (LULUC) .....	56
5.3.1	Features Selection /(PCA) .....	56
5.3.2	Features Classification /(K-SVM) .....	60
5.4	PERFORMANCE ACCURACY (AC) .....	65

5.4.1	PCA Performance .....	65
5.4.2	Features Extraction Performance -LULCC .....	69
<b>6.</b>	<b>CONCLUSIONs AND FUTURE WORK .....</b>	<b>76</b>
6.1	ANALYSIS OF RESULTS .....	76
6.1.1	Fundamental of Water Extraction Analysis.....	77
6.1.2	Analyze the Evaluation of Water State Results.....	78
6.1.3	Features Extraction Analysis .....	79
6.2	CONCLUSIONS .....	80
6.3	FUTURE WORK .....	81
	<b>REFERENCES.....</b>	<b>82</b>

## LIST OF TABLES

	<u>Pages</u>
Table 1.1: Description of Data Set .....	19
Table 3.1: Data set .....	31
Table 3.2: Performance comparison between methods .....	41
Table 3.3: Performance of MMO method .....	41
Table 4.1: Evaluated areas of MWL over years .....	49
Table 4.2: Areas of water quality classes .....	50
Table 5.1: Classes Identification and areas.....	64
Table 5.2: Eigenvectors Matrix for TM data for the year 1986.....	66
Table 5.3: Eigenvectors Matrix for TM data for the year 1987.....	66
Table 5.4: Eigenvectors Matrix for ETM <sup>+</sup> data for the year 2000/April .....	67
Table 5.5: Eigenvectors Matrix for ETM <sup>+</sup> data for the year 2000/December .....	67
Table 5.6: Eigenvectors Matrix for OLI data for the year 2017/April .....	68
Table 5.7: Eigenvectors Matrix for OLI data for the year 2017/December .....	68
Table 5.8: Eigenvalues for all data set.....	69
Table 5.9: Calculated area for classes over years .....	70
Table 5.10: Assessment accuracy for classification approach.....	71

## LIST OF FIGURES

	<u>Pages</u>
Figure 1.1: Location map for the study areas .....	17
Figure 2.1: Elements of remote sensing.....	22
Figure 2.2: The radiation components to contribute the water intensity .....	23
Figure 2.3: The structure of representing satellite Image .....	24
Figure 2.4: Diagram for one level DWT input image decomposition .....	28
Figure 2.5: Diagram for SVM linear and nonlinear separable.....	29
Figure 3.1: Flow chart for preprocessing.....	30
Figure 3.2: Preprocessing Chart for input data .....	35
Figure 3.3: NDWI With segmented Threshold.....	36
Figure 3.4: One level Decomposition for the input image.....	37
Figure 3.5: Water area coastline extracted from (HL) .....	37
Figure 3.6: Extracted water area with GWT .....	38
Figure 3.7: Processing steps of water surface by (MMO) .....	39
Figure 3.8: Estimated graph for water surface areas.....	42
Figure 4.4.1: Enhanced color composite images for all Landsat's data .....	44
Figure 4. 2: Reservoir area extraction (RAE) for the enhanced images .....	46
Figure 4.3: Water Quality Classification .....	48
Figure 5.1: Flowchart for PCA processing .....	59
Figure 5.2: Features selection (RGB) pcs images.....	60

Figure 5.3: Hybrid classification Process .....	61
Figure 5.4: Hybrid classification process for TM of 1986 and 1987 years .....	63
Figure 5.5: Hybrid classification process for ETM <sup>+</sup> of 2000/Apr and 2000/Dec years.....	64
Figure 5.6: Hybrid classification approach for OLI data for the year 2017/Apr,2017/Dec.....	64
Figure 5.7: Estimated graph for distinguishing the areas over years .....	70
Figure 5.8: Distribution areas for each class over years .....	73
Figure 5.9: Distribution classes areas for each proposed year .....	74
Figure 6.1: Clip part shows water surface receding.....	78

## LIST OF ABBREVIATIONS

MD	:	Mosul Dam
MDR	:	Mosul Dam Reservior
ETM+	:	Enhanced Thgematic Mapper
OLI	:	Operational Land Imager
TM	:	Thematic Mapper
USGS	:	U.S Geological Survay
SWIR	:	Shortwave Infrared
RS	:	Remote Sensing
DN	:	Digital Numbet
IFOV	:	Field of View
WT	:	Wavelet Transform
Pixels	:	Picture Elemnts
NDWI	:	Normalized Difference Water Index
DWT	:	Discrete Wavelet Transform
SVM	:	Support Vector Machine
LULC	:	Land use Land Cover
DIP	:	Digital Image Processing
NIR	:	Near -Infrared
RGB	:	Red,Green,Blue
ROA	:	Region Of StudyArea
WSE	:	Water Surface Extraction

GWT : Gabor Wavelet Transform

MMO : Mathematical Morphological Operations

MSE : Mean Square Error

PSNR : Peak Signal to Noise Ratio

OBA : Extracted Object Area

SR : Segmented Region

MWL : Monitoring Water Level

RAE : Reservoir Area Extraction

MWQ : Monitoring Water Quality

Ed : Euclidean Distance

AC : Performance Accuracy

Pa : Producer Accuracy

Ua : User Accuracy

$K^{\wedge}$  : Kappa Coefficient

LULUC : Land use Land cover Classification

PCA : Principal Component Analysis

HIS : Intensity, Hue and Saturation



# 1. INTRODUCTION

This chapter presents general information about the study area location, illustration for the data that had implemented, main outlines of this work and the objective.

## 1.1 DESCRIPTION OF STUDY AREA

Mosul Dam(MD) considered as one of the significant water resources projects that constructed in the north of Iraq in the year of 1981 on the Tigris river , which is considered one of the two important rivers in western Asia, and its flows from the Hazar Lake that located in the south eastern region of Turkey [1]. The Dam operation that implemented with primer filling of reservoir was on July 1986 [1].

Mosul Dam Reservoir (MDR) is one of the biggest manmade lakes on the Tigris River in the north of Iraq around 60 km northwest of Mosul city from the borders of Syria and Turkey, as showed in Figure1.1 [2].The shape of it is elongated where the Tigris river inflows and expand near to dam location[1][3]. Furthermore, it is located between latitude ( $36^{\circ}36'N$  - $36^{\circ}50'N$ ) and longitude ( $42^{\circ}27'E$  -  $42^{\circ}58'E$ ). The surface area of the lake is approximately 385 km<sup>2</sup>. It has a storage capacity of about 11.11 km<sup>3</sup> and is located 330 meters above sea level.[2][4].

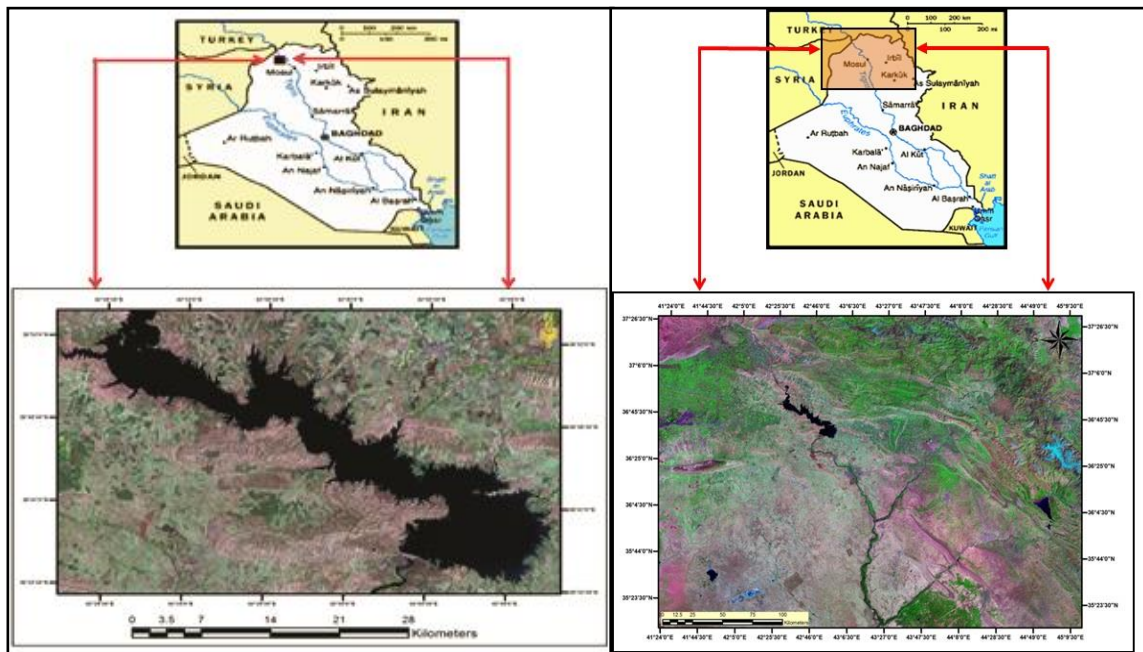


Figure 1.1: Location map for the study areas

## **1.2 MATERIAL AND DATA SET**

The remote sensing data represented by satellite images are the most significant resource used for testing various land cover features.[5] In this work, different remote sensing data for satellite Landsat images were chosen for various dates for the two seasons through the 31 years, specifically from (1986-2017), to locate changes which occurred in the water surface of Mosul dam reservoir. Input satellite images were captured from the U.S. Geological Survey website (USGS),[6] as mentioned in Table 1.1.[7][8] It is worth noting, the thermal bands' spatial resolution used in Landsat's was (120x120) meter, (60x60) meter, and (100x100) meter respectively. However, their product resampled to (30x30) meter, thus obtaining an accurate estimation of the water area, according to the following site (<https://landsat.usgs.gov/what-are-band-designations-landsat-satellites>) .[9]

## **1.3 DESCRIPTION OF DATA SET**

Landsat is a joint effort of the U.S. Geological Survey (USGS) and the National Aeronautics and Space Administration (NASA). NASA develops remote sensing instruments and the spacecraft, then launches and validates the performance of the instruments and satellites. The USGS then assumes ownership and operation of the satellites, in addition to managing all ground reception, data archiving, product generation, and data distribution Second paragraph[10].

This work performed various types of Landsat's that carried on different sensors in various seasons, such as Landsat-5 which carried on Thematic Mapper(TM), Landsat-7 that carried on Enhanced Thematic Mapper Plus(ETM+), and Landsat 8 which carried on the Operational Land Imager (OLI) sensor [11].

TM sensor consist of visible and additional bands which located in the shortwave infrared (SWIR) part of the spectrum, improved spatial resolution of 30 meters for the visible, near-IR, and SWIR bands, and the addition of a 120-meter thermal IR band. Delivered Landsat 5 TM thermal data are resample to 30 meters as mentioned in table 1.1 [7].

**Table 1.1:** Description of Data Set [7]

Landsat Type	Capture date of data	Bands Name	Spectral resolution ( $\mu\text{m}$ )	Spatial resolution(m)
Landsat 5 TM	22/ April /1986	Band1 blue	0.45–0.52	30 m
		Band2 Green	0.52–0.60	30 m
		Band3 Red	0.63–0.69	30 m
	23/ October /1987	Band4 NIR	0.76–0.90	30 m
		Band 5 SWR1	1.55–1.75	30 m
		Band 7 SWR2	2.08–2.35	30 m
		Band 6-TIR	10.40–12.50	120 resampled to 30 m
Landsat7ETM <sup>+</sup>	22/ April /2000	Band1 blue	0.45–0.52	30 m
		Bnad2 Green	0.52-0.60	30 m
		Bnad3 Red	0.63-0.69	30 m
	23/Dec/2000	Band4 NIR	0.77–0.90	30 m
		Band 5 SWR1	1.55–1.75	30 m
	20/April/2002	Band 7 SWR2	2.08–2.35	30 m
		Band 6-1-TIR	10.40–12.50	60 m resampled to 30 m
		Band 6- 2 TIR	10.40-12.50	60 m resampled to 30 m
		Band8- Panchromatic	0.52-0.90	15 m

Landsat8 OLI	20/April/2015	Band 1-ultr	0.43–0.45	30 m
	22/ April /2017	Band2 blue	0.45–0.51	30 m
		Band3 Green	0.53–0.59	30 m
	23/December /2017	Band4 Red	0.64–0.67	30 m
		Band5 NIR	0.85–0.88	30 m
		Band6-SWIR1	1.57–1.65	30 m
		Band7-SWIR2	2.11–2.29	30 m
		Band8- Panchromatic	0.5-0.68	15m
		Band9-Cirrus	1.36-1.38	30m
		Band10-Thermal Infrared(TIRS)1	10.60-11.19	100m
	Band11-Thermal Infrared(TIRS)2	11.50-12.51	100m	

Landsat 7 carries the Enhanced Thematic Mapper Plus (ETM+), with 30-meter visible, near-IR, and SWIR bands; a 60-meter thermal band, and a 15-meter panchromatic band. Delivered Landsat 7 ETM+ thermal data are resampled to 30 meters (table 1.1). Landsat 8, launched as the Landsat Data Continuity Mission on February 11, 2013, contains the push-broom Operational Land Imager (OLI) and the Thermal Infrared Sensor (TIRS). OLI collects data with a spatial resolution of 30 meters in the visible, near-IR, and SWIR wavelength regions, and a 15-meter panchromatic band, which provides data compatible with products from previous missions. OLI also contains a deep blue band for coastal-aerosol studies and a band for cirrus cloud detection[7].

#### 1.4 MAIN OUTLINES

The aim of this thesis is to examine the efficiency of using temporal remote sensing data for detecting and monitoring the water case in Mosul Dam reservoir over a period of time. The

structure of this thesis demonstrates as the following: Chapter 1 starts with giving a brief illustration about the location of study area and general information for input data and the objective of research. In Chapter 2 background and literature review explained for first part. In the second part characteristics of Landsat's that used in this work will be demonstrated. In Chapter 3, description for water body extraction through various image processing methods. In Chapter 4 water reservoir quality and level changes are implemented .In Chapter 5, applying the changes that occurred over time period for different features that are located around the reservoir by implementing Land use Land cover hybrid classification (LULC). Finally, chapter 6 clarifies discussion and analysis of extracted results, and then concludes the work of thesis.

## **1.5 OBJECTIVE AND ACHIVMENT OF WORK**

Iraq is facing water shortage problem in the last years due to climate changes and higher human life demand for the water [12]. MDR is the biggest structure was built on Tigris River to provide water for useful life related to saving electricity and tourist location. Therefore, it is necessary to evaluate the variations that occurred on its water quality and storage level through the period from its first constructed until 2017. Thus, this can help the scientists for water resources to recognize the dangerous of reduction of water in the reservoir. According to that, this study aims to achieve the following objectives:

- 1- Comparing between different techniques to detect the coastline of reservoir to estimate the changing of cover water area with best technique.(conferees paper)
- 2- Determining the changing of water level and storage.
- 3- Applying the effect of sedimentation which enters from Tigris River during its flow to reservoir on its water quality.
- 4- Evaluate the changes that affected on the features around the reservoir due to environmental changes that were lead to variation of the covered area with water in reservoir.

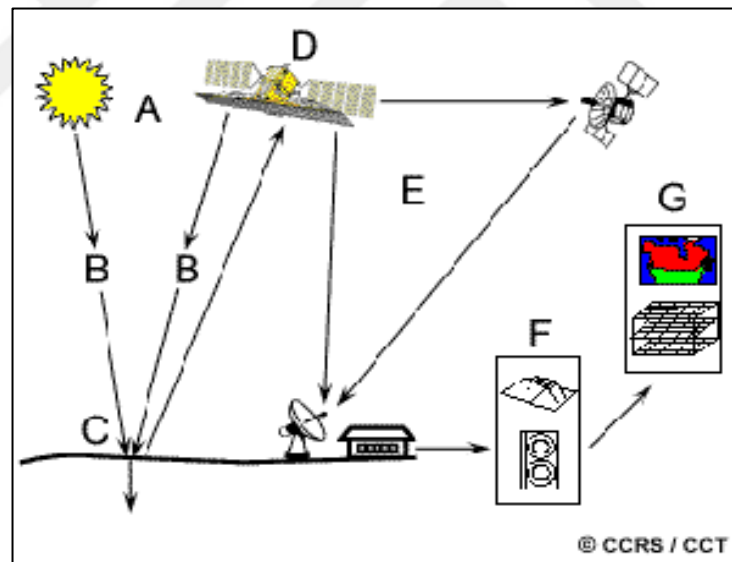
To achieve the mentioned objectives MATLAB codes were utilized by implementing temporal remote sensing data as mentioned in table 1, and performing different image processing techniques which gain the objective of this work properly.

## 2. BACKGROUND

This chapter demonstrates identification of remote sensing and its impact for water monitoring, remote sensing and image processing, overview of Landsat's, and literature review.

### 2.1 BASIC OF REMOTE SENSING

Remote Sensing(RS) has been defined in several ways, one of them described remote sensing is a science , art and technology that observed different objects on the earth from far way distance without physical contact with any of objects [13]. This is done by sensing and recording reflected or emitted energy and processing, analyzing, and applying that information. Such as, this process involved an interaction between incident radiation and the targets of interest through seven elements as explained in figure2.1,[14] . In other word, this interaction based on the electromagnetic radiation energy and the object[15] .

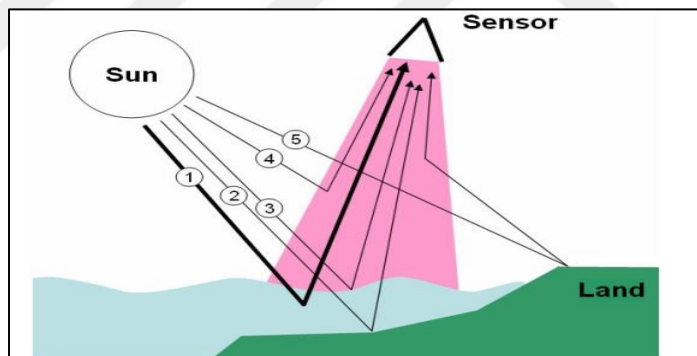


**Figure 2.1:** Elements of remote sensing

Where, (A)the energy source, (B) Radiation and the Atmosphere,(C) Interaction with the Target,(D) Recording of Energy by the Sensor,(E) Transmission, and Processing, (F) interpellation and analysis, and (G)[14], is the final element which represent the application that needed from the acquired objects for different fields of study .

### 2.1.1 Remote Sensing in Water Resources

RS has significant role to solve different issues related to water resources that which involve coastal and fresh water bodies, such as(rivers, lakes and derange patterns)[16].With the development of new sensor technologies its became more prospective to monitor different features from land cover simultaneously and rapidly. Thus, water quality has estimated excessively by using remote sensing techniques[17]. This estimation has been affected by the intensity and spectral radiation which created from the sun and propagates through the atmosphere , then into water through the interface between air- water as described in figure 2.2 Whereas, the pink color represent the reflected radiance from water to sensor , and 1,2,3,4, and 5 assimilate the steps for water radiation , such as (1) is the upwelling from the water,(2) which reflected from the bottom,(3) the interface that reflected between air-water,(4) that scattered to sensor by atmosphere between water and sensor, and (5) the radiation that reflected from the target to sensor [18].



**Figure 2.2:** The radiation components to contribute the water intensity

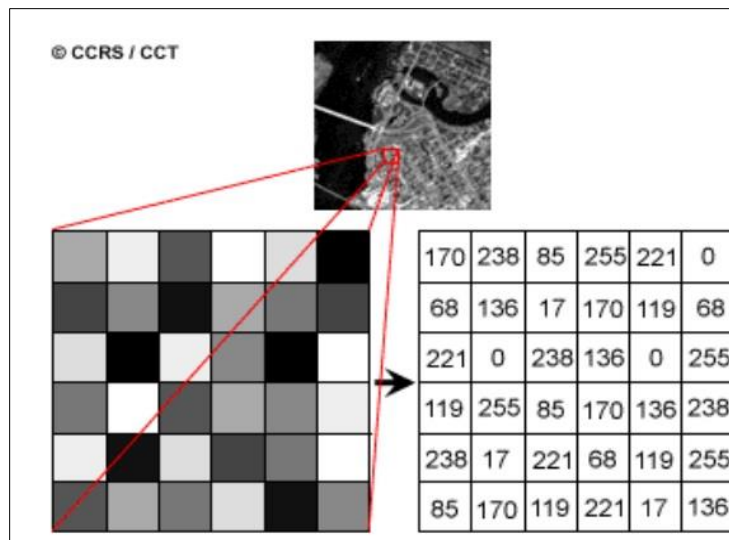
It's clear that RS techniques measure the water surface changes by spectral signature and wavelength reflectance. Thus, the reflection of water is be more strong in short wavelength with blue or green-blue reflected color in visible radiation, and in near infrared or red it appeared dark [14]. as well as the optimal wavelength which used for water quality measurement.[19]. To improve water quality comprehensive information related to water source and water management is needed. Landsat satellite images provide rich knowledge to the scientists who are interested working in water management and agriculture[20].

### 2.1.2 Representing Landsat Satellite Data

According to the input data that implemented in this work which are utilized different satellites data (images), it's necessary to explain basic concepts related to how these remote sensing images are represented to be suitable and clear for users in various fields of study.

There are two terms extracted from the electromagnetic energy reaction in remote sensing applications, images and photographs. That is to say, the recorded electromagnetic energy from remote sensing devices represented graphically to create an image. When these images recorded as photographic film specifically that time they called photographs[14]. Based on these definitions we can say to all photographs are images.

The information that are detected from the electromagnetic energy with different wavelengths as mentioned in Figure 2.1 and in the analyzing and interpretation step are recorded in digital format to represent digital image as showed in figure 2.3[14] , which is possessed from sets of picture elements called pixels that describe the objects of captured areas by dividing it into equal squares in size which depended of the satellite characteristics regarded to the spatial resolution[21], and each pixels contain a Digital Number (DN) which illustrates the intensity that reflected from each object[14][22] .



**Figure 2.3:** The structure of representing satellite Image

In most RS applications multiple images (bands) are utilized as implemented in this work, by offering a multispectral input data sets with multiple bands with different wavelength[6] [22]. Furthermore, dealing with multiple bands obtain more information about the features (objects) of



the study area with different wavelengths rather than using single band with one narrow wavelength and poor information [23][6]. That is lead to gain high performance of the investigated results.

## **2.2 SPECTRAL RESOLUTION**

Satellite images (bands) distinguish various objects or features such as, water, vegetation, and different types of rocks by comparing their responses regarded to different range of wavelength and identify each feature with different colors which describes its reflectance .This is called spectral resolution[14] Furthermore, its describe the capacity of sensors to differentiate the objects according to the best wavelength intervals[24]. The range of wavelength determines the precision of spectral resolution for any feature. That is to say, the narrow wavelength range the obtained finer spectral resolution for features[14].

The reflected colors in visible part of the spectrum represented with (Red, Green, and Blue) and the features detected according to these colors with different wavelength range.[13]

Many remote sensing systems record energy over several separate wavelength ranges at various spectral resolutions. These are referred to as multi-spectral sensors. And advanced multi spectral sensors called hyper spectral sensors which are describe the features with high spectral resolution, due to detecting hundreds of narrow spectral bands throughout the visible , near-infrared, and mid- infrared portion of the electromagnetic spectrum. This provide very high spectral resolution for distinguishing various types of features easily[14].

## **2.3 SPATIAL RESOLUTION**

In the satellites sensor system a spatial resolution describes the information in the acquired image by meters that different from Landsat's to demonstrate the amount of details which are be visible to human eye[21]. In other word, it gives the ability to recognize the features and distinct.

The satellite images (bands) vary by their size of spatial resolution. Such as the input data of this work almost all types has 30 meters spatial resolution for visible, 60 , and 120 for thermal .However all spatial resolutions had been processed to 30 meters[7] as mentioned in Table 1.2 which mean the size of each pixel in an image equalize to square of 30 meter (30x30) on the ground that let even small features when evaluating the features in an image with their Instantaneous Field of View (IFOV).

Images in all remote sensing collected form a two dimension (2D) matrix that partition the image into squares of picture elements (pixels) which describe the value of spatial resolution of the sensor. For instance in our work the spatial resolution is 30 meters , each pixel represents the area on the ground by a square of (30x30) meters [14]. Therefore , there is no difference between spatial resolution and pixel size in satellite images,[21]

## **2.4 LITERTURE RIVEW**

Remote sensing is considered one of effective tools that distinguish different types of patterns on the earth. Furthermore, it's a practical way to detect the temporal changes that occurred in the water bodies (rivers, lakes) due to environment changes by evaluating their surface extension. The surface extension has been evaluated with implementing various types of image processing methods that concerned on water body extraction.

This section clarified the previous studies which dealt with the methods and algorithms that implemented in this study.

### **2.4.1 Normalization Difference Water Index Method (NDWI)**

NDWI its one of well-known methods that detect most types of water surfaces suggested by [25] McFeeters to detect water surfaces in wetland environment and measure water surface dimension from Landsat TM by finding the ratio between band 2 and band 4. The modified NDWI was proposed by [26] to enhance water information which appear mixed with built-up land in the area of extracted water.

Furthermore [27] clarified the NDWI for the water areas that derived from temporal Landsat7 ETM data for seven month to demonstrate the case of soil surface water content and leaf water content of the vegetation during growing seasons. In [28] using NDWI with other methods to extract wetland features by using different satellites and implementing bands algebras through utilizing ERDAS software. The NDWI implemented in [4] for automatic delineation of the Mosul Dam lake coastline from satellite image.

## 2.4.2 Wavelet Transform (WT)

WT became one of the well-known theories in last decades which provide a mathematical form to multiresolution representation in most of texture analysis for remote sensing applications and many other applications in signals and image processing[29]. Furthermore, it has ability to provide a time and frequency representation for the signal in a decomposition process[30].

### 2.4.2.1 Discrete wavelet transform (DWT)

DWT has property to analyze the information of two dimensional signals (2D) which represented with an image in a less cost of computation time by using filtering techniques. It decomposes the signal into two parts coarse approximation and detail information[29].

DWT utilize two types of functions, scaling and wavelet functions that related to low pass and high pass filter bank successively. As described in figure 2.4[30]. These properties increased (WT) theory importance and utilizing (DWT) in image fusion as a best approach through decomposed two images with different resolution[29]. Furthermore, (WT) theory has proved its effectiveness for extracting features from hyperspectral data by transforming it from original space to a scale space plane[30].

In [9] WT based in contour let which provide spatial and spectral information of image by using Laplacain pyramid method .The extension to the 2-D WT (two-Dimensional) is performed by using a product of 1-D WT (one Dimensional). In practice the image transform is clarified by applying a separable filters bank to the input image that represented with low pass and high pass filters. Thus, DWT as demonstrated in this section decomposed the original input image by a set of sub-images at several scales which describe a multiscale analysis for the input image that provide easier information related to objects of image. In other word, each sub image includes information about the specific scale and orientation regarding to separable filter bank in both raw and column directions[31] as displayed in figure 2.4. Whereas, H and L mentioned to Low pass and High pass filters respectively.  $\downarrow 2$  denotes the down sampling (decrease the sample occurrence rate) by a factor of two. In practice with the image the 2-DWT decompose it to four sub images that represent the information of original pixels as well as the neighboring pixel values with different frequencies low(L) and high(H) respectively.

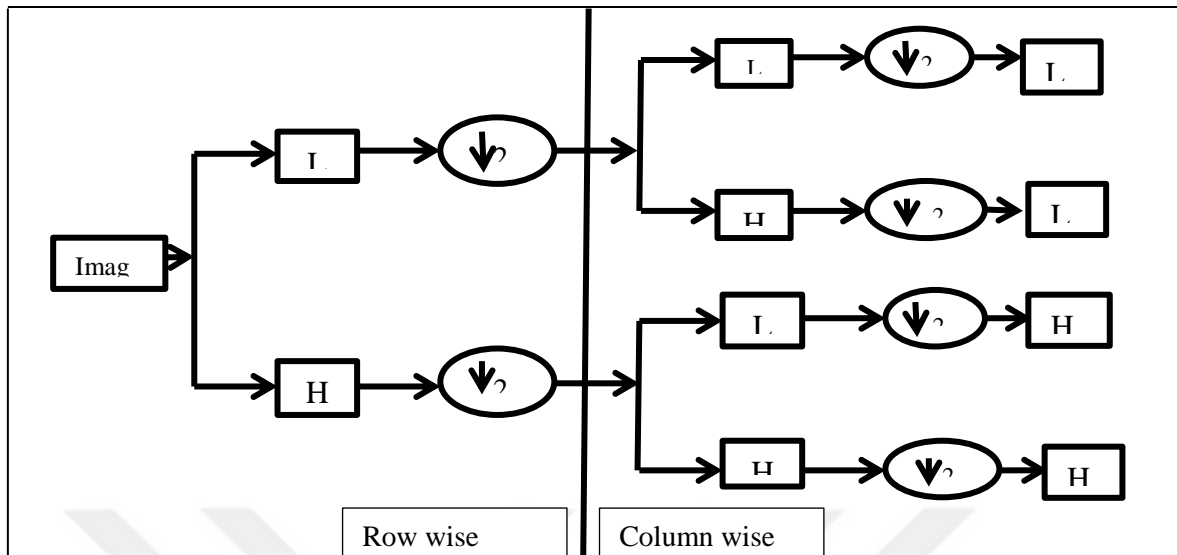


Figure 2.4: Diagram for one level DWT input image decomposition

### 2.4.3 Morphological Techniques

Morphological technique gives an approach to deal with features in an image according to their geometrical shape, its developed by J. Serra and G. Matheron [32]. morphological techniques are incorporated with remote sensing data for detecting features specifically the edges and noise reduction comparing with filters[33]. A new segmentation method was proposed regarded to morphological method by implementing pixel similarity between connected features depending on the morphological distinguishing of features in an image [34].

### 2.4.4 Classification

#### 2.4.4.1 K-Means clustering

This method represent one of the well-known unsupervised classification methods which is split the pixels in an image to the number of classes regarded to their reflectance[35]. Therefore, it's widely used in remote sensing applications for land cover and pattern recognition. The performance of applying unsupervised K-means clustering algorithm for features and texture extraction of remote sensing data improve the high classification accuracy assessment which based on clustering with K-means by using various distance calculations to classify land cover features[36]. Furthermore, K-means clustering algorithm used to classify high resolution satellite images into spatial groups related to segmentation approach[37]. Implementing filters (LOG and Prewitt) in such incorporated with k-means to detect the different types of building from satellite images proposed in [38].

### 2.4.4.2 Support vector machine (SVM)

SVM is a supervised classifier that developed in machine learning approach with to the framework of the statistical learning theory by each of V. Vapnik and co-workers in 1995[39]. Furthermore, SVM vastly applied in remote sensing land cover classification based on specifying the location of decision boundary to get the best isolation of the classes based on the statistical theory and the state of SVM and the classes[40].

SVM was introduced to apply binary for two classes to distinguish, however in case of dealing with multiple classes to classify in most remote sensing images, as we implemented in this work this need a multiple classes methodology that provide SVM expanded to solve nonlinear decision surface through generating  $n$  classifiers, where  $n$  is the number of classes figure 2.5[41]. The final output is the class that corresponds to SVM with the largest margin by two approaches (one against one and one against rest) [40][35]. According to that SVM was applied for reliable land characterization, and feature extraction from RS images through segmentation process [41] .

The SVM approach seeks to find the optimal separating hyperplane between classes as shown in Figure 2.5[41] by focusing on the training cases that are placed at the edge of the class descriptors. This way, not only is an optimal hyperplane fitted, but also less training samples are effectively used; thus high classification accuracy is achieved with small training sets. This feature is very advantageous, especially for remote sensing datasets and Image Analysis, where samples tend to be less and less in number[42].

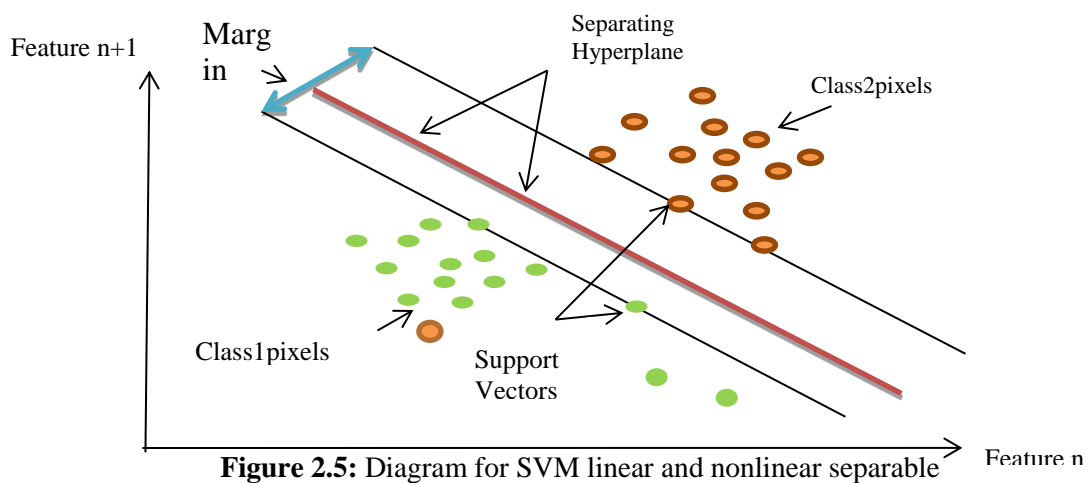


Figure 2.5: Diagram for SVM linear and nonlinear separable

### 3. WATER SURFACE EXTRACTION VIA IMAGE PROCESSING TECHNIQUES

RS data has significant impact for earth surface studies in different fields. Such as, water surface studying, Land use land cover (LULC) classification, environment affect , climate changes , and monitoring temporal changes for all features[15].

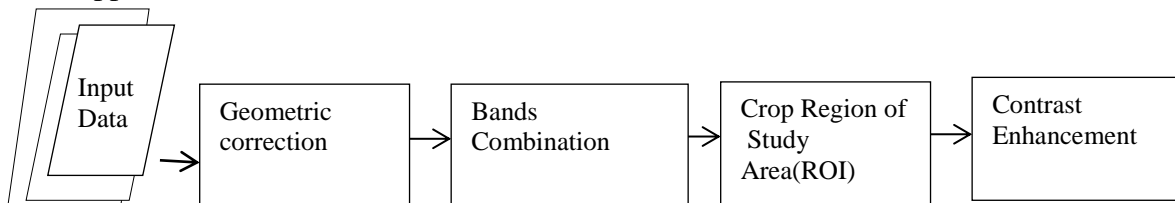
Digital image processing (DIP) has efficiency to compound with RS data to implement the objective of any study. This chapter demonstrates DIP techniques which had been implemented through MATLAB coding to extract the coastline of MDR and parts from the Tigris River through its entering to Mosul city, and evaluate the temporal changes due to environmental impacts.

#### 3.1 METHODOLOGY FOR WATER EXTRACTION

To apply the processing methodology of this work, there are two significant steps should be conducted. The first one is preprocessing, which includes preparing the images In order to be more appropriate in subsequent operations as shown in figure 3.1. Noticing that this step will be performed for all further processing that will be mentioned in the following chapters Where the second is clarifying a coastline detection through utilizing different DIP techniques then estimation the water body area integrated with efficiency of temporal RS images to distinguish the changes that take place in water surface areas in Mosul city between the periods of years (2002-2015).

#### 3.2 IMAGE PREPROCESSING

The preprocessing is very important in RS applications, and its essential step related to all satellite images beforehand any application for the image will be applied. Its includes sequential operations as shown in figure 3.1 which are essential for image to be more suitable for the desired applications[43].



**Figure 3.1:** Flow chart for preprocessing

### 3.2.1 Input Data Set

Two types of satellite input data were used for processing in this section: three bands of Landsat-7 (ETM+) data, and three bands of Landsat-8 (OLI) data. table 3.1 which includes a description of the input data[6] [44][6] that selected from table 1.1. All images (bands) were obtained from the US Geological Survey (USGS) website and are suitable for detecting water surfaces [23].

**Table 3.1:** Data set [7]

Satellite type	Capture date	Bands Wavelength (um)	Spatial resolution (m)
Landsat-7 ETM+	April, 2002	Band 1: 0.45-0.515	30x30 m
		Band 3: 0.63-0.69	30x30 m
		Band 4: 0.77-0.90	30x30 m
		Band 5:1.55-1.75	30x30 m
Landsat-8 OLI	April, 2015	Band 2:0.452 - 0.512	30x30 m
		Band 4:0.636 - 0.673	30x30 m
		Band 5:0.851 - 0.879	30x30 m

### 3.2.2 Geometric Correction

RS images exposed to geometric distortion during the acquisition time by the system ,the skew of the platform, scan skew and due to mirror scans This caused displacement of the features in an image[43]. In this work due to we deals with characteristics of the objects in an image and their peers in the ground truth it is essential to applied this step .Therefore, geometric corrections are applied to correct the inconsistency between the location coordinates of the raw images(input data) and the real coordinates on the ground or base image[43].

The implemented method based on transforms the raw satellite input data to a portrait form. To do this, mathematical form was utilized in MATLAB through implementing a general affine transformation expression  $R^2$  is defined by  $M: R^2 \rightarrow R^2$  , and expressed by the following equation [45].

$$(I, J) = M(L, N) \quad (3.1)$$

Where, M is the affine transformation, which transforms set of (L,N) of input data ,  $R^2$  to set of (I,J) ,  $R^2$  the Orth-rectified out images. This demonstrate how to obtain pixel from input image and put it in output image with identical location, by using reverse transformation which expressed as pair of polynomials, as following equations [45].

$$I = Q(L, N) = q_0 + q_1L + q_2N + q_3LN \quad (3.2)$$

$$J = R(L, N) = r_0 + r_1L + r_2N + r_3LN \quad (3.3)$$

We get polygonal image that represent the Orth-rectified out image. In order to obtain the exact matching we perform a rotation for the a polygonal image which represent the ROI by angle ( $\emptyset$ ) to achieve exact projection that tend all objects are be compatible with base ground images [43][45].

### 3.2.3 Bands Combination

RS data composed from different bands, each of them are distributed in a specific range related to electromagnetic spectrum[6]. Applying bands combination aims to make the processing of all Landsat data more valuable, through utilizing multiple bands to represent RGB composites image from three bands which has the ability to display one feature with different colors and distinguish different features in original input data that have same spectral characteristics such as water surfaces that mixing with plants and building are complicated to distinguish as water with single band [46].

In our work multiple bands related to water reflectance appearance were used to extract water surface areas be visually seen in visible and near-infrared bands[47]. Based on that ,a suitable bands combination that applied , such as using near-infrared (NIR) and shortwave infrared (SWIR) showed a very distinct difference across aquatic and terrestrial land cover types and produced an accurate image of the whole water areas[48]. According to that, multi-bands (5,4,1) were combined to obtain a true color composite image of ETM+ and(5,4,2) in OLI which gain more and clear information as well it indicted to easier interface between land features and water surface [49][23]. Whereas, band 1 in various Landsat's represented with blue normal color which is suitable for water studying due to its high reflectivity for the water through its wavelength [23] ,while in Landsat 8(OLI) band 2 perform the same purpose [11]regarding to the same wavelength of band 1 in ETM+ . Therefore, we utilized combined bands (5,4,1) for ETM+ data and (5,4,2) Furthermore, using band-5 (shortwave- infrared) as Red channel and band-4 (near-infrared) as Green channel are showed the best contrast between water and land features [49][50].Then , color image enhancement was implemented to enable a satisfactory conversion of the relief features in the RGB, in clearly combined images [20]. Notice that the output



preprocessed images will be used to represent input images for the following processing that is applied in this work.

### **3.2.4 Crop Region of Study Area (ROA)**

The cropping approach is a big challenge for the size and dimension of RS data. Furthermore, the huge land cover features that are obtained from RS data include rich information which cause the detection and monitoring for the specific feature is more complicated[51].

In our study, we concentrate to extract the water surface areas from input data, Thus, the geometrical images were cropped due to avoid time consuming through processing. Whereas the size of original image is row (X) and column(Y), and the range of cropped image varies in both the row and column, such as the range of column different from minima of left- top, left -bottom to maxima of right top to right bottom. The range of row different from the minima of top-left, bottom- left to maxima top-right, bottom right. In MATLAB its implemented by Crop-image(X1:X2, Y1:Y2)[52].

### **3.2.5 Contrast Enhancement**

Contrast enhancement is one of the most important features of the image enhancement technique i.e. it manipulates the illumination level of the image[15].

Image enhancement method was implemented to enable a satisfactory conversion of the relief features in the RGB color composite images to clarify clear view[20]. Furthermore, a contrast image enhancement has performed to redistribute the gray level of the color RGB image after convertint it to gray for easier process to the whole range. That was led to increasing the intensity of pixels for all levels with more brightness and improved the interpretability of the information that presents in an image [53].

## **3.3 WATER SURFACE EXTRACTION (WSE)**

In the recent years the estimation of water body from RS data has occupied a significant domain in many fields related to water resources studies, such as, management, monitoring, wetland detection, and Lake Coastline extraction, due to climate changes that affects clearly in water cycling. Furthermore, remote sensing image processing field is a solution how to evaluate temporal information about water in order to

develop the strategies to control flood calamities as well as the characterizations of land and water surface temporarily [46],[54].

In this section various DIP techniques combined with RS data were applied to detect WSE for different areas. According to that, two approaches had implemented in this section. The first one, utilizing RS input data for the sensor ETM<sup>+</sup> as mentioned in table 3.1 to extract the coastline of MDR, through implementing three multiple bands which are suitable for water resources studying[6], and combined together to extract one composite color image based on comparing between three methods. The second approach include extracting WSE which related to different areas covered with water in Mosul city represented with Tigris River during its flow in Mosul city, MDR, and small swamps by using temporal RS data between the years (2002 -2015) by using ETM<sup>+</sup> and OLI sensors to evaluate the variation that occurred in storage space of water surface areas. Consequently, three multiple bands were chosen as clarified in table 3.1, such as (5, 4, 3) bands for ETM<sup>+</sup> and (5, 4, 2) for OLI sensors based on implementing Morphological operation method.

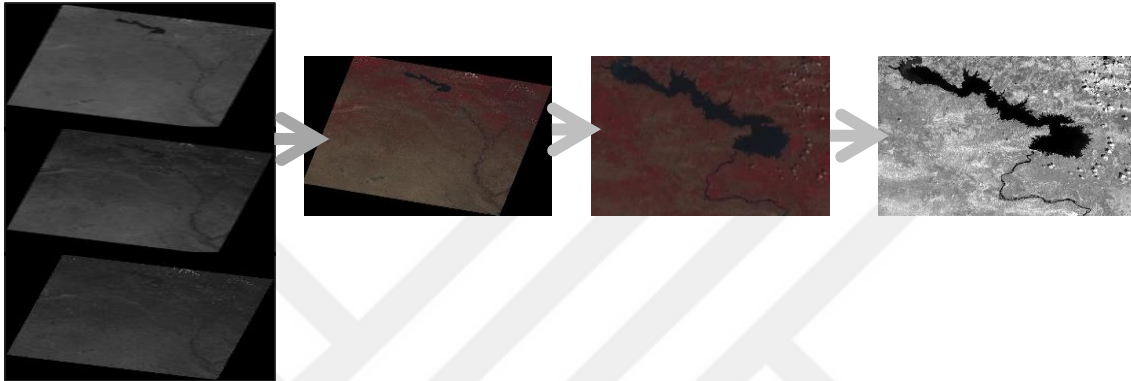
### **3.3.1 Reservoir Coastline Extraction**

The coastline represented by line such as edge that separate between water mass and the land, its ground feature that specified the shape and location of water areas and land use[4]. RS images used to distinguish this line integrated with DIP techniques[14]. This section represents a comparative study between different DIP methods that extract the coastline for MDR. That is to say, there will be a comparative performance between the implemented methods.

As clarified in section 3.2 that clarified preprocessing steps as showed in figure 3.1, A combination between these 3 bands has done to gain (RGB) true color image which gives clear interface between land and water [49], Furthermore (band 5, near infrared) represented with(R) channel is the best for extraction land and water interface, and also it exhibits a strong contrast between land and water features due to the high degree of absorption of mid infrared energy by water [50]. In addition to, that main Characteristic of rivers can be seen optically in visible/near infrared remotely sensed data (bands) [47].

After true colored image had been extracted, that leads to obtain a good indication of land/water. Furthermore, the differences of wavelength between combined bands have an effective impact for distinguishing different features[55]. In order to get more accurate result with less execution

time, cropping operation has implemented for getting specific part with more cleared features [49]. Last step of preprocessing was contrast enhancement after converting cropped image to gray one. That is to say, image enhancement has done to increase the intensity of pixels for all levels with more brightness and improved the interpretability of the information that present in an image[15][56].



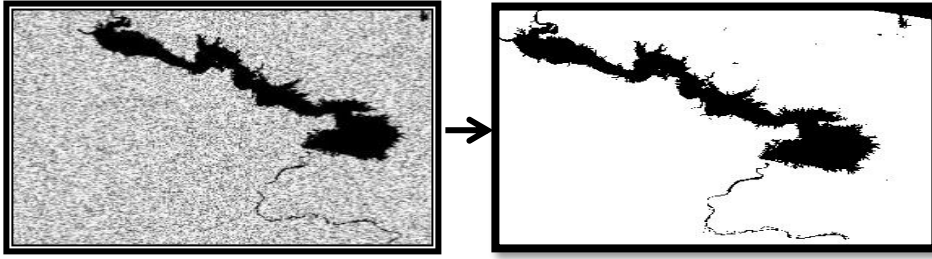
**Figure 3.2:** Preprocessing Chart for input data

### 3.3.1.1 Normalized difference water extraction (NDWI)

Many of spectral water indexes have been developed to extract water body from RS data[57]. NDWI consider one of the most important methods that detect water surface, It has been suggested by McFeeters since 1996 to detect surface water in wetland environment and measure water surface dimension, [58][25]. It is defined the ratio between two suggested image bands by calculating the normalized differences between them[57]. In this section the developed NDWI method normalized difference moisture index (NDMI)[59] was utilized to detect the coastline by calculating the ratio between band4 near-infrared (NIR) and band5 middle-infrared(MIR) were chosen for this section as clarified in Equation (3.4).

$$NDMI = \frac{(B4-B5)}{(B4+B5)} \quad (3.4)$$

Thus, NIR preferred for extracting the coastline and water body extraction due to it has strong absorption by water, also both NIR and MIR has higher ability to distinguish between water areas/land areas. This lead to obtain high capacity of the output extracted image as shown in figure 3.2 based on selecting a manual threshold to remove any mixing pixels between water and land [58].



**Figure 3.3:** NDWI With segmented Threshold

### 3.3.1.2 Wavelet transform (WT)

The characteristics of RS multispectral data which regarded to both spatial and spectral features are correlated with bands[31]. WT is a key solution for this problem through presenting input data in both spatial and spectral frequency domain with multiresolution analysis for the signal[9]. Thus, WT is a mathematical tool deals with images in multiresolution. Furthermore it can be represented by the following equations[60].

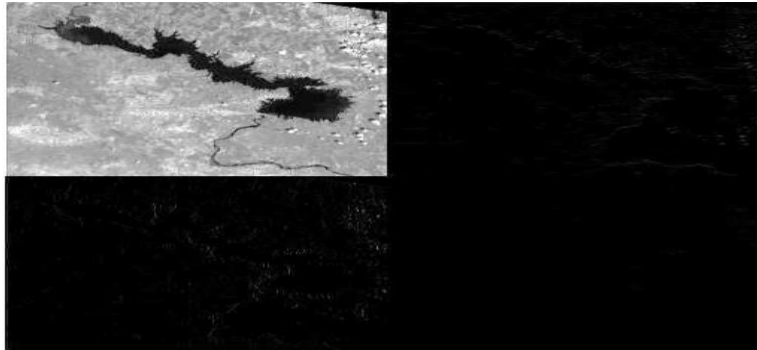
$$F(w) = \int_{-\infty}^{\infty} f(t) e^{j\omega t} dt \quad (3.5)$$

$$C(\text{Scale}, \text{Position}) = \int_{-\infty}^{\infty} s(t) \varphi(\text{Scale}, \text{Position}, t) dt \quad (3.6)$$

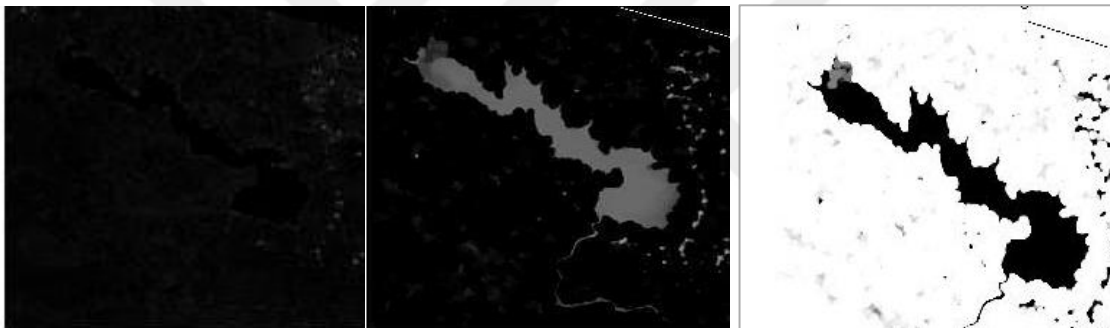
Where, C are the coefficients from WT results, and  $\varphi$  is the wavelet function of scale and position[60]. Consequently, in recent years WT became a significant tool for processing RS images that had non stationary behavior through local variation in orientation and frequency for features texture depending on multiresolution scale for the images.[31][61]. That is to say, one level decomposition of the 2-DWT was implemented in this work by using Haar wavelet. Based on that, decomposing the ETM<sup>+</sup> Landsat input image after preprocessing operations decomposed to four sub-images as mentioned in figure 3.3. Among them, one contains the WT coefficients in low frequency range called the approximation part LL that includes most useful information with high resolution and three high frequency range in three directions: vertical (LH), horizontal (HL) and diagonal (HH) called the detail parts that performed the edges [31].

The extraction of the coastline was clarified in approximation part (LL). However, there were different features around the coastline in the LL .Whereas, In vertical part (HL) the edge of border that separate the water surface of reservoir can be seen with representing the edge of input image [62]. So, depending on this approach we utilized this property to obtain the coastline regarding to its edge not directly from the approximation part (LL) that part would be depended

in most studies interested in wavelet. Based on this, by subtraction operation this part from the background of the input image had been applied, then clear unwanted features around the water area by using segmented threshold [63] as seen in figure 3.4 .



**Figure 3.4:** One level Decomposition for the input image



**Figure 3.5:** Water area coastline extracted from (HL)

### 3.3.1.3 Gabor wavelet transform (GWT)

Gabor Filter has clear influence for decreasing noise and has good capacity to enhance the extracted features[62]. Furthermore, Adding Gabor to remotely sensed images suppress the noise and gain more specific extracted features that related to the different orientation of Gabor filter[64]. Gabor wavelet transform has the properties of multi-resolution and multi- for measuring local spatial frequencies that lead to consider it a popular method for feature extraction[50].

Consequently, The two dimensional Gabor-Wavelet filter has been applied which removes noise with less time consuming. However, WT could extract both the time (spatial) and frequency information from a given signal(image) GWT has some impressive mathematical properties through applying on the image with different orientation at different scale which increase the clearness of extracted features more accurate. Thus, in this section combining GT with DWT As

shown in figure 3.5 suppress the noise and has gain more specific extracted features that related to the different orientation of Gabor filter through clearing the border of coastline without need to segmented threshold[50].



**Figure 3.6:** Extracted water area with GWT

### 3.3.2 Mathematical Morphological Operations (MMO)

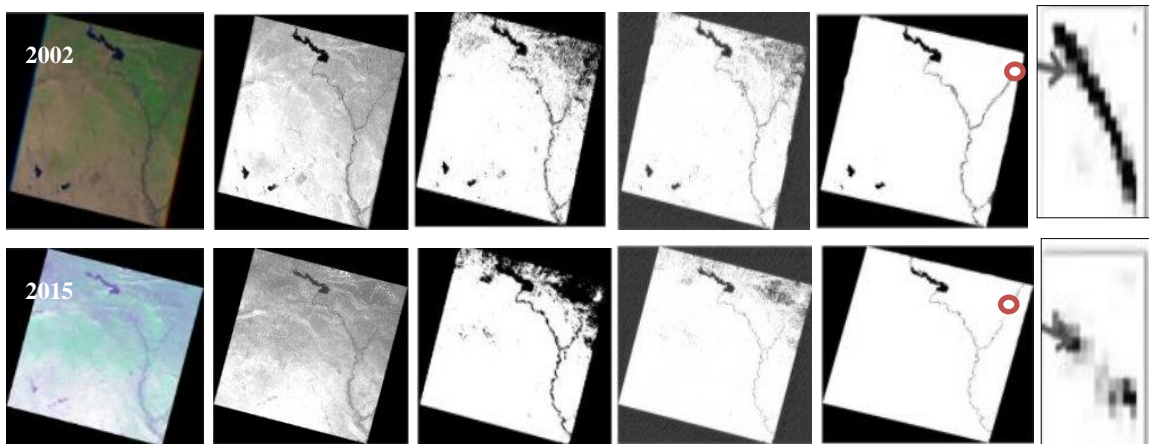
MM operations have significant approach in distinguishing water surfaces and differentiate between water areas and land features accurately[63]. This section published in IJEEE SCIE , [105].

Temporal RS data integrated with DIP had implemented to estimate the changes that occurred in the water surfaces between the years (2002-2015) from the images obtained from the sensors ETM<sup>+</sup> of the year 2002 and OLI of the year 2015 as described in table3.1 The applied methodology of this section based on implementing a morphological operator which contained in the toolbox of MATLAB library through DIP applications to detect the objects (water surfaces) which will then afterward be extracted.

After applying preprocessing for the input images and obtain one combined enhance image for each year binarization for the gray image is the first operation which applied through this section to improve the quality of extracted objects[33]. To do so, an adaptive global threshold method which assimilate the best and simplest segmenting method that convert gray image to new binary one regarding to its proposed value that predefined [65], [66] to distinguish the water areas by calibrating the pixels of the gray image with the threshold value ( $T=0.75$ ) which used to test the gray images. That is to say, each pixel value in gray image greater than the threshold value ( $T$ ) it becomes one (1) in out binary image else it becomes zero(0). Due to, the reflection of water in satellite images represented by black pixels (zeros) the whole areas that covered with water detected clearly. Then, two significant morphological operations erosion and dilation which

clarified the state of any given pixel in the output image by applying a rule to the corresponding pixel and its neighbors in the input image[67]. This rule based on denoting a relation between input image and arbitrary structuring elements with kernel size (5x5) which is utilized in this section.

Consequently, to perform the erosion of a binary image, we successively place the center pixel of the structuring element on each foreground pixel (value 1). If any of the neighborhood pixels are background pixels (value 0), then the foreground pixel is switched to background. Furthermore, to perform dilation of a binary image, we also successively place the center pixel of the structuring element on each background pixel. If any of the neighborhood pixels are foreground pixels (value 1), then the background pixel is switched to foreground. That denotes to obtain a new out binary image which extracted the boundaries of all water surface areas, as showed in figure 3.6. However, there were still tiny mixed pixels that distributed randomly around and through the water areas that caused noise as a well unclean boundary for water surface areas. Therefore, the median filter has particularity for removing the outliers pixels without changing the shapes in the out binary images, [32][68]. That is led to obtaining the segmented objects of areas that covered with water clearly.



**Figure 3.7:** Processing steps of water surface by (MMO)

### 3.4 PERFORMANCE CRETERIA (AC)

The objective performance and assessment accuracy are significant in the processing of DIP and RS applications. To analyze and calibrate the effectiveness of implemented processing[69] through applying statistical calculations to improve the performance of the methodology.

According to that, this section divided the calculations in two parts regarded to processing which implemented to extract WSE. That is to say , in section 3.3.1 three methods were performed to

extract the coastline of MDR ,the performance calculated through two criteria's to gain which method has highest performance with less error .

Consequently, Mean Square Error (MSE) equation 3.7and Peak Signal to Noise Ratio (PSNR) equation 3.8 were utilized to find the performance of implemented methods and improve their effectiveness for coastline extraction by obtaining high performance through PSNR and less error value MSE which almost nonexistent as clarified in table 3.2 .

$$MSE = \frac{\sum_{JK}[N1(j,k)-N2(j,k)]^2}{J * K} \quad (3.7)$$

$$PSNR = 10 \log_{10} \left( \frac{R^2}{MSE} \right) \quad (3.8)$$

Where in equation3.7, J, K represents the dimension of images, and N1, N2 represent the images before and after processing respectively. In addition to, R<sup>2</sup> in equation 3.8 represents the gray level range for the images (0-255)[69].

The performance of any methodology estimated by utilizing statistical calculations regarded to the determined objective. Thus, in section 3.3.2 the performance is based on statistical measurements, as displayed in table 3.3 b by calculating the accuracy based on the object of the extracted water surface areas for the out results images. Thus , the accuracy is measured using equation (3.9) [70],[7].

$$AC = \frac{OBA}{TOA} * 100 \quad (3.9)$$

Where, *OBA* the extracted object area which is defined water surface areas in this work and is measured by equation (3.10), *TOA*: Total number of pixels for reference need original image( input Landsat data).

$$OBA = \sum_{n=1}^m SR \quad (3.10)$$

Where *SR* : the segmented region object of water surface areas per pixels .

According to a number of water surface areas which were segmented through MM method, the area regarding to water pixels was measured by equation (3.11),[71] .Thus , each pixel represented by a 30x30 meters [72].

$$SR = \frac{pr}{pn} * A \quad (3.11)$$



Where,  $p_r$ : the pixels of segment need water surface objects area,  $p_n$ : is the number of pixels not related to water the surface and  $A$ : is the scale factor for square area.

To clarified that a spatial resolution of input satellite images for each pixel was equalized to 30 meter which means each pixel on satellite images represented by the square  $30 \text{ m}^2$  in the field location.[7][72] Accordingly, the segmented area of water surface for each year calibrated in ( $\text{Km}^2$ ) unit as mentioned in the following mathematical expressions.

$$\text{Rating}(\text{Segmented water objects}) = (30 * 30) * \text{No. of black pixels}$$

$$\text{Area}(\text{Km}^2) = \text{Rating}(\text{metres})/1000$$

**Table 3.2:** Performance comparison between methods

ETM+ combined image	Proposed Criteria's	Water coastline proposed Methods		
		NDWI	WT	GWT
	MSE	0.0142	0.0034	0.0021
	PSNR(dB)	42.52	48.71	50.20

Through MSE and PSNR that clarified in table 3-2 to prove the optimal technique or method that applied to extract the coastline of MDR. Whereas, MSE unit as clarified in equation (3.7) measure the processing error between the original image and the resultant image. Consequently, GWT method obtain less error and high PSNR as explained in equation (3.8) Which gives the amount of clarity of the resulting image and is inversely proportional to the MSE value[21].

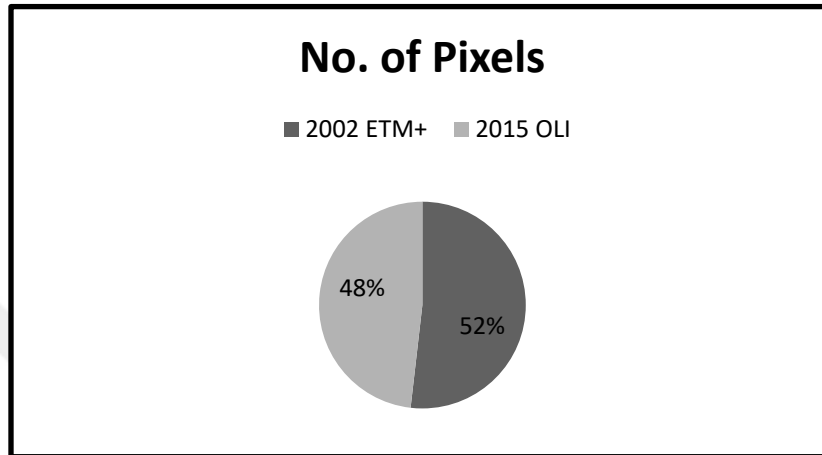
**Table 3.3:** Performance of MMO method

Satellite type	Capturing date	No. of pixels for water surface	Area rate in $\text{km}^2$	Object-based accuracy
ETM+ landsat-7	April 2002	240384	7.211 $\text{km}^2$	91.699%
OLI Landsat-8	April 2015	223485	6.704 $\text{km}^2$	85.252%

Another performance criterion to evaluate second phase for this section through implementing MMO method clarified in table 3-3 according to equations (3.9),(3.10) and (3.11) object based accuracy and for segmented water surface areas calculated , in addition to, the area rate applied in ( $\text{km}^2$ ) to evaluate the differences in the areas that covered with water over years .

In order to reinforce the out result of section 3.3.2 which clarified the changes of the occupied areas the covered of water surface over (13) years, figure 3-7 demonstrate the graph of areas regarding to the number of water pixels which obtained for each year by using Excel software graph.

Consequently, its noticed from figure 3-7 the areas that covered with water for 2002 year of ETM Landsat data has 52% while the same areas acquired 48% in the 2015 year of OLI Landsat input data.



**Figure 3.8:** Estimated graph for water surface areas

That confirms that the areas covered by water has been declining in recent years because of sudden climate changes and the lack of standards of rainfall[2] compared to previous years and according to the current study, which dealt with the 13 years period.

## 4. EVALUATION OF WATER STATE

Water resources consist of coastal water bodies and fresh water bodies (lakes, rivers)[16]. RS applications combined DIP techniques have essential issue to monitoring water state (WS) parameters such as water quality and water level storage.

This chapter clarified the applications of DIP through different RS data and describes how these technologies integrated to be benefit tools for evaluating and monitoring WS. Since the past few decades due to environmental and climate changes which indicate degradation of water level and quality due to climate and environmental changes over years that impact on Tigris River flow through its entering to Iraqi territory , which is provide MDR with water.

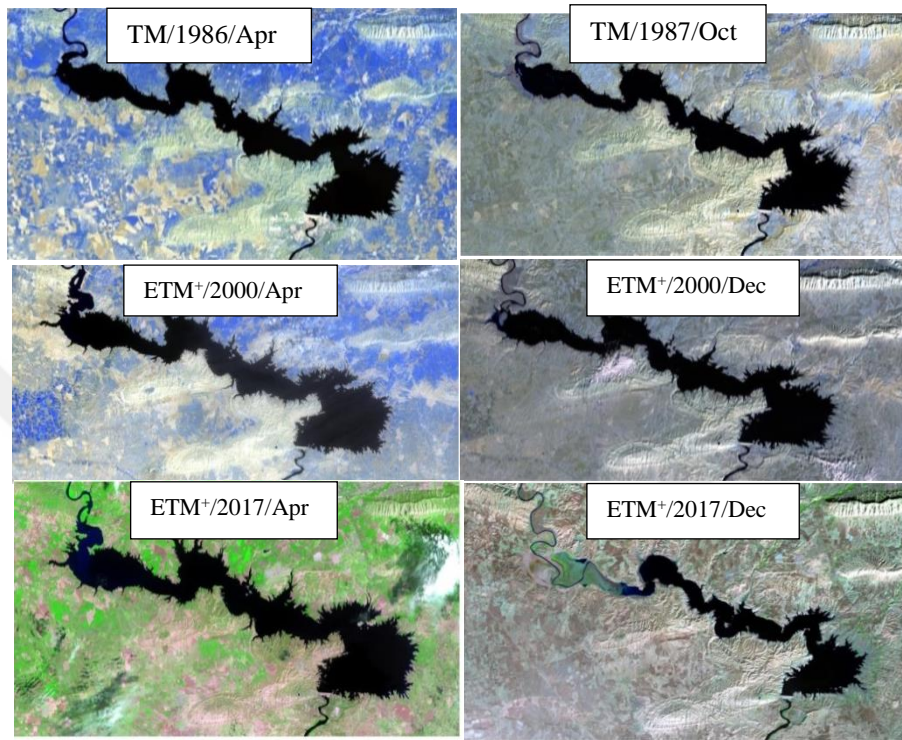
According to the methodology that applied in this chapter, we concentrate on studying water state of MDR over time specifically the period between the years (1986-2017), which is considered one of the most significant lakes that established on Tigris River due to its tourist strategic location and saving electricity [73] .

This based on, utilizing temporal RS data. Thus, different satellite Landsat images were chosen as clarified in table 1.1for various dates for the two seasons through the 31 years specifically form (1986-2017) years period to locate changes which occurred in the water surface of MDR. Input satellite images were captured from the U.S. Geological Survey website (USGS),[6] . It is worth noting, that spatial resolution for thermal bands' which used in Landsat's was (120x120), (60x60), and (100x100) meters respectively. However, their product resembled it to (30x30) meter, thus obtaining an accurate estimation of the water area, according to the following site (<https://landsat.usgs.gov/what-are-band-designations-landsat-satellites>). This led to use thermal band through combination without sampling its resolution with other visible bands[23].

### 4.1 MONITORING WATER LEVEL (MWL)

RS techniques have been widely utilized in monitoring water level assessment[20]. As mentioned in section 3.2 preprocessing operations performed on the Landsat's images for the years 1986-2017 as described in table 1.1 by chosen (7,5, and4) for bands combination approach which converted then into RGB composite enhanced images for each year as shown in figure 4.1. Mentioned that choosing the bands NIR=4, SWIR1=5, and SWIR2=7, for obtaining

composite image showed a very distinct difference across aquatic and terrestrial land cover types, and produced an accurate image of the lake[48].



**Figure 4.1:** Enhanced color composite images for all Landsat's data

The results of enhanced images as mentioned in figure 4. 1 plain of the most prominent features around the lake that resulting in performing the objective of this section which estimate the variation in storage level of water in MDR since the year of its construction specifically in the year of 1986 over 31 years To do this, region of interest (ROI) implemented from the enhanced images to extract the area of reservoir.

#### **4.1.1 Reservoir Area Extraction (RAE)**

A significant approach to coastline detection is to differentiate between water areas and land features. Most of the previous researches followed either the Normalized difference water method or digitization[4][58][74] to extract the coastline. In this work, hybrid bands combination were performed to obtain the region-body of the lake area. As seen in figure 4.2. The hybrid bands combination were applied to isolate and segmented the region area (ROI) of the reservoir. The hybrid method based on combination between the bands (7,5,4) that already combined in section 4.1 with the bands (1,2,3) that utilized for the input data of October of the year1987, and

December of the years 2000, 2017 sequentially. In the other hand, bands (7, 5,4) hybrid with the bands (1, 6 and 3) which has picked from input data in the April of the years 1986, 2000, and 2017. Those bands combination had chosen separately, due to variations in terms of capturing seasons and the variation in characteristics of Landsat's (TM, ETM, and OLI)[7].

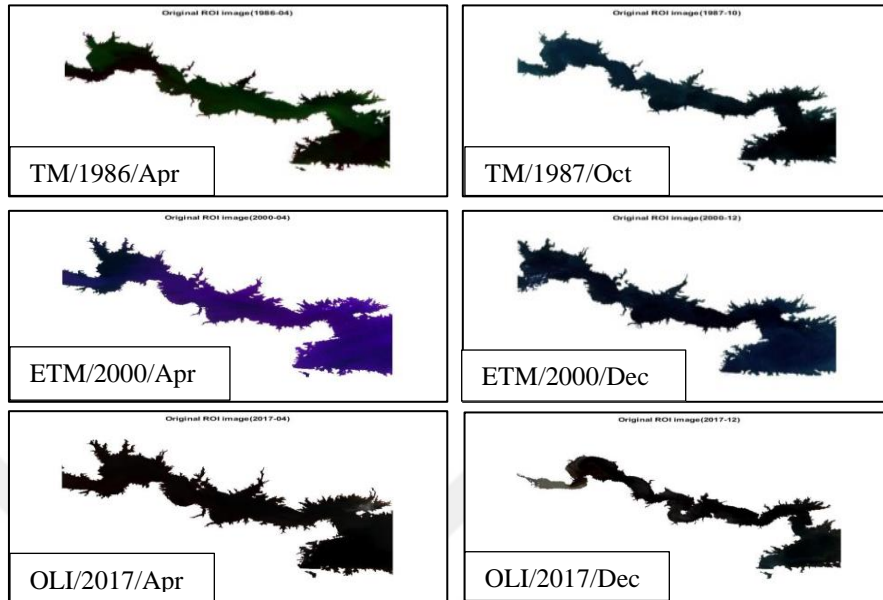
Furthermore, using thermal bands from both Landsat-5 and Landsat-7 via hybrid band combinations reinforced the accuracy of the results for extracting the water area on processing due to their produced resolution to 30 meter and to calibrate the result images that extracted from OLI which has 12-bit resolution and its limitation for detecting water. (<https://landsat.gsfc.nasa.gov/precious-resources-water-landsats-thermal-band/>),[7].

## **4.2 MONITORING WATER QUALITY (MWQ)**

Many Studies refers to MWQ as process which used RS utility as good tools to analyze and identified the characteristics of water bodies such as chemical, biological and physical[16]. Our work interested in studying MWQ through turbidity, clarity , color tone and sediment which indicate to physical characteristics[16]. Based on that, water reflectance changed over the years due to its composition and elevation level.

Generally, clear water appears black or dark blue in the band combinations of the composite images[75] .Moreover, variations in the color of the water, seen in figure 4.2 (dark black, light black )or near to grey and green color[76]) caused different water reflectance due to sediment accumulation from the Tigris River's water flow as it pours into the lake, and also from climate change during rainy seasons[73].

Consequently, the purpose of this section is to detect the variation in the lake water quality, which has been associated with its water level elevation over the years. Note: the differences in constituent pixels of water reservoir were distinguished according to their reflectance[77] In addition to, there is a variation in the chromatic gradient of the water's base color over the years. According to that, classification methods unsupervised and supervised had been used in this section to recognize the variation in the reflectance for water lake pixels that changed over years due to sediment distribution which enters from Tigris River to the MDR and results in quality of its water.



**Figure 4. 2:** Reservoir area extraction (RAE) for the enhanced images

The extracted areas for each input data in figure 4-2 clarified segmentation for MDR in such way explain the variation of covered area of reservoir for each proposed input data. Thus, the difference in space area related to the disparity of water level over years [6], this will be detailed by a statistic graph in the section of performance accuracy for calculating MWL areas for implemented data.

#### 4.2.1 Hybrid Classification

Combined classification algorithms were used in most land cover studies to improve the advantages of each selected algorithm.[78] The combined algorithms were selected in this section to perform pixels variety from extracted lake area images as displayed in figure 4.2 which contributed to classifying the lake's water quality. An unsupervised clustering k-means and supervised support vector machine (SVM) algorithms were used, respectively.

Unsupervised classification or clustering process pixels were identifying and gathered with regard to their same spectral reflectance then collected into groups that labeled classes[79][106]. Moreover, through the algorithm in this study noticed that the identification of prior information about the variation of the pixels intensity in the lake water area can be recognized [80], despite, the classification algorithm including collection features that have the same spectral characteristics groups of classes. The unsupervised k-means algorithm in this section used to

identify the differences in pixels intensity in the lake water that consider as one class with regard to the land cover classification and separate that difference into categories of classes according to their centroid which represented by calculating the mean of each pixel in cluster as showed in in Eq.4.1,then collect each cluster regarding to measuring the closeness to the center by applying the Euclidean distance between pixels, equation4.2 [81],[82].

Consequently, three clusters were selected randomly (k=3) in the implemented program trying to detect three labeling clusters, due to lake water pixels intensity reflectivity [83].

$$Cp(p1(x, y), p2(x, y), \dots, pK(xn, yn)) = \left( \frac{\sum_{i=1}^k p1}{K}, \frac{\sum_{i=1}^k p2}{K}, \dots, \frac{\sum_{i=1}^k Pnthi}{K} \right) \quad (4.1)$$

Where, Cp: centered pixels of K<sup>th</sup> cluster in N<sup>th</sup> dimensional of all pixels .

$$Ed = p(xi, yi) \sqrt{\sum_{i=1}^N (xi - yi)^2} \quad (4.2)$$

Where, Ed Euclidean distance between pixels, N: total number of pixels.

However, some pixels were gathered into the cluster with misclassification problems. In other word, classes were not completely isolated during statistical iterations[78]. Therefore, a supervised support vector machine (SVM) has hybridized with k means to correct the misleading information and implemented the regularization of the pixels in each class[80]. Furthermore, SVM has nonparametric properties, which maximizes the margin between classes[35], all these properties draw the attention for applying SVM in remote sensing applications for classification through extracting an appropriate hyperplane between classes[39], through a basic binary classification approach to multi SVM classes classifier form[80][106]. Thus ,in this work non linearly separable classes through multi SVM classifier has applied due to rectify the confusing information that obtained from k-means clustering results, which means dealing with more than two classes, to improve its property of dealing with separable data by testing a combination of some of the binary classifications, where remarked one in the current class for instance, and other classes were zero [80] . According to that , the hyperplane forms for training the input data which called support vector as described in equation 4.3,[39] and clarified in chapter 2 in figure 2.5 has extended in such a manner that makes it effective in separating the boundaries of classes linearly by adding the parameters (C and  $\gamma$ ) which they had defined once to linear kernel K(x, y)



to maximize the margin between the hyperplanes as shown in equation 4.4 [39]. The out results in figure 4.3 showed the hybrid classification process to distinguish the quality of water in MDR through three classes and the variation in each class over 31 years period.

$$y_i(w \cdot x_i + b) - 1 \geq 0 \quad (4.3)$$

Where:  $(x_i, y_i)$  Training samples,  $w$ : the norm to the hyperplane and  $b$  is the basis

$$y_i(w \cdot x_i + b) \pm C \sum_{i=1}^r \gamma \quad (4.4)$$

$\gamma \geq 0$ ,  $C$  regularization value.

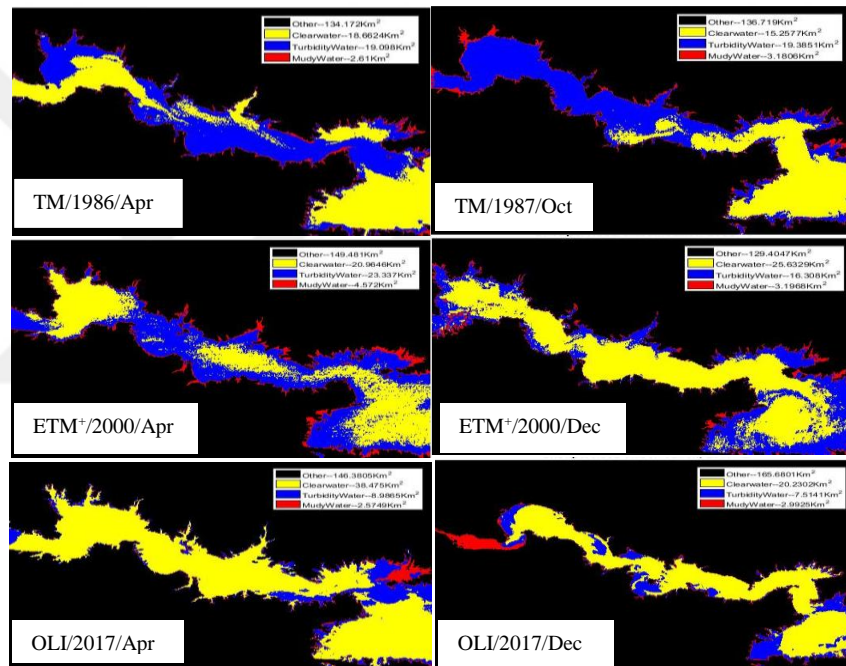


Figure 4.3: Water Quality Classification

The classification process extracted three classes that were suggested through classification process and described the quality of water in MDR with different areas rates over years In other word, figure 3-4, clarified label classes for MWQ such as pure ,turbidity and muddy with yellow, blue and red colors respectively and the rate area for each class as will be clarified in next section through evaluation the performance of processing for MWQ.

### 4.3 PERFORMANCE ACCURACY (AC)

As clarified in section 3.4 performing the performance improve the efficiency of the work and implemented methodology. Thus, section 4.1 MWL for used Landsat's of different years had



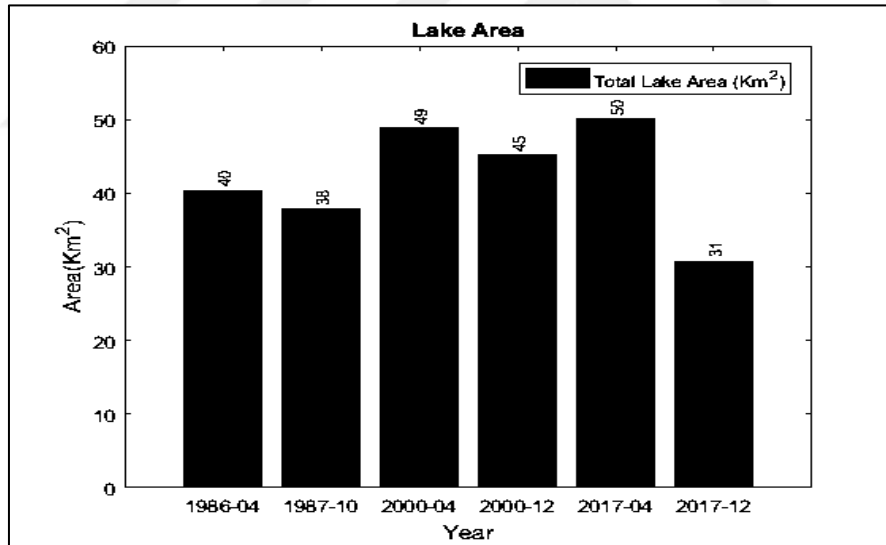
been extracted through RAE detection to represent ROI for this work stage. Based on that, the variation in storage of water area was measured for calibration with the actual lake area storage values (per Km<sup>2</sup> unit) to evaluate these changes between the seasons. Thus, a spatial resolution of input satellite images for each pixel was equalized to (30 x 30) m, which means each pixel on satellite images represented 30 square meters in the ground field[7][72]. Accordingly, the estimated values for MWL for the reservoir surface for each year measured in (Km<sup>2</sup>) as clarified in figure 4.4 by counting the zeros pixels which identified the water level of lake areas for input data as clarified in section 4.1.1, by applying equations (4.5) and (4.6).

$$ROI = \frac{RA}{TA} * A \quad (4.5)$$

$$\text{Rating (ROI)} = (30*30) * \text{No. of black pixels} \quad (4.6)$$

Lake Area (Km<sup>2</sup>) = Rating (meters)/1000.

Where *RA*: pixels of extracted region, *TA*: pixels not related to water, *A*: scale factor of squared area.



**Figure 4.4:** Estimated graph for MWL over years

Furthermore, the performance of MWL is applied statistically by calculating the assessment accuracy (*Acc*) of the MWL method. Thus, finding the ratio between segmented water areas to whole input image, as expressed in equation (4.7)[69].

$$Acc = \frac{\sum_{k=1}^M Dij}{Tp} \times 100\% \quad (4.7)$$

Where: *Dij* is the sum of classified pixels, *Tp* is the total number of all pixels.

**Table 4.1:** Evaluated areas of MWL over years

Input data and Landsat's	Total Area of Water level(Km <sup>2</sup> )	Overall Accuracy(Acc)
April 1986 TM	40 Km <sup>2</sup>	97.1717%
October1987 TM	38 Km <sup>2</sup>	99.197%
April2000 ETM <sup>+</sup>	49 Km <sup>2</sup>	98.9973
December2000 ETM <sup>+</sup>	45 Km <sup>2</sup>	99.126%
April 2017 OLI	50 Km <sup>2</sup>	97.691%
December 2017OLI	31 Km <sup>2</sup>	97.2083%

In addition to, the performance of MWQ section 4.2 applied by calculating the area of each class as clarified in equations 4.5 and 4.6 that demonstrated in table 4.2. figure 4.5.

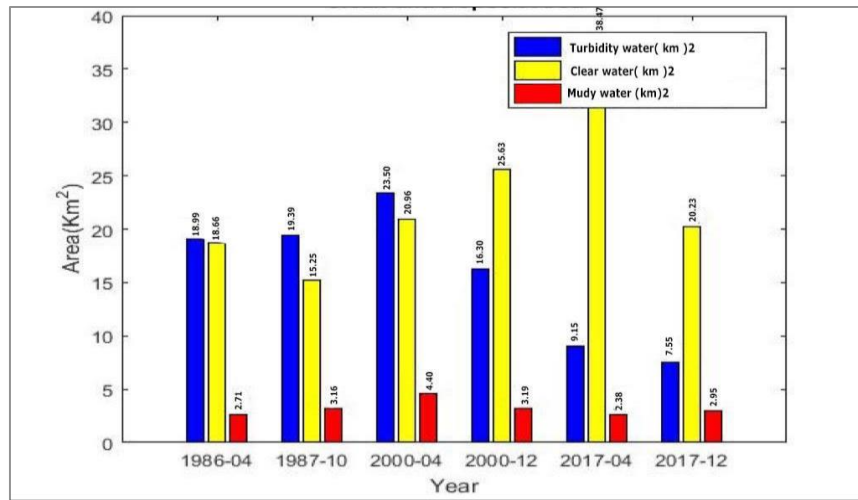
Thus, figure 4.5, clarified the statistic graph that illustrate the variation which found in the areas of water classes that presented in table 4.2 over the years.

**Table 4.2:** Areas of water quality classes

Captured date of data and Landsat's	The local area of water lake classes Km <sup>2</sup>		
	Pure	Turbidity	Muddy
TM ,April, 1986	18.6624	18.9927	2.7171
TM ,October, 1987	15.2577	19.3968	3.168
ETM <sup>+</sup> ,April, 2000	20.9646	23.5053	4.4037
ETM <sup>+</sup> ,December, 2000	25.6329	16.3008	3.1932
OLI ,April, 2017	38.475	9.154	2.3814
OLI ,December, 2017	20.2302	7.5528	2.9538

This table clarified extracted classes areas for input data , as illustrated in section 4.2.1, That is to say, three classes distinguished from MDR , as seen in table 4-2 the rates had different values between classes over years whereas pure class has maximum values in rate when the direction of water towards to reservoir depth. However, the sedimentation from Tigris River through entering to the reservoir [12]. Therefore, the turbidity class detected and muddy class it can be detected in the areas near to the coastline of reservoir. In other word, muddy areas which are located between land and water [7].

Consequently, the disparity for the extracted classes over proposed years clarified in figure 4-5 , Thus, it can be seen from the graph that the maximum value of pure class and minimum value of muddy class shows in the shows in the year 2017/April .



**Figure 4.5:** Estimated graph for water classes areas over years

Another performance criteria that evaluate the effectiveness of classification process is assessment accuracy which depended on statistical calculations [90]. Since, a confusion matrix (error matrix) the most common form for implementing the assessment accuracy (AC) of classification result. From this matrix we can extract several measures of classification accuracy can be calculated, including percentage of pixels correctly classified, errors of omission, errors of commission and Kappa Coefficient of Agreement.

That is to say, the overall accuracy (Acc) clarified the percentage of categories that calculated by dividing the sum of the diagonal entries of the error matrix by the total number of reference pixels as demonstrated in equation (4.7). In addition to, the nondiagonal values in each column represent errors of omission and nondiagonal values in each row represent errors of commission. In other word, errors of omission for each category are computed by dividing the sum of incorrectly classified pixels in the nondiagonal entries of that category column by the total number of pixels in that category. Also, errors of commission for each category are calculated by dividing the sum of incorrectly classified pixels in the nondiagonal entries of that category row by the total number of pixels in that category [84].

Furthermore, measuring errors of omission and errors of commission accuracy related the Producer accuracy (Pa) and User accuracy (Ua) respectively [84], [85]. And the Individual class accuracy that calculated by dividing the number of correctly classified pixels in each class by either total number of pixels in the corresponding column, which denoted by Producer accuracy (Pa) as clarified in equation (4.9) and Users' accuracy (Ua) calculated in the same manner with the only difference being that the total number of correctly classified pixels for a category is divided by the total number of pixels in that category in the row marginal or row total

instead of dividing by the total number of pixels in the column marginal or column total as clarified in both equation(4.8), (4.9)[85] [69]. As seen in table 4.3.

$$Ua = 100\% - \frac{\sum Di}{D_i} \% \quad (4.8)$$

Where:  $Ua$  is the sum of classified pixels in each row,  $Di$  is the total number in the row.

$$Pa = 100\% - \frac{\sum Dj}{D_j} \% \quad (4.9)$$

Where:  $Pa$ : sum of classified pixels in column,  $Di$  is the total number in column.

Another measurement unit is the Kappa Coefficient ( $K^{\wedge}$ ) is a discrete multivariate measure that differs from the usual measures of overall accuracy assessment in basically two ways. First, the calculation takes into account all of the elements of the error matrix, not just the diagonals of then matrix (Foody 1992). This has the effect of taking into account chance agreement in the classification. The resulting Kappa measure compensates for chance agreement in the classification and provides a measure of how much better the classification performed in comparison to the probability of random assigning of pixels to their correct categories[80].

The Kappa Coefficient of Agreement,  $K^{\wedge}$ , is calculated as following equation (4.10)[84].

$$K^{\wedge} = \frac{N \sum_{i=1}^r X_{ii} - \sum_{i=1}^r (X_{i+} * X_{+i})}{N^2 - \sum_{i=1}^r (X_{i+} * X_{+i})} \quad (4.10)$$

Where:

$r$  = the number of rows in the error matrix

$X_{ii}$  = the number of observations in row  $i$  and column  $i$

$X_{i+}$  = the marginal totals of row  $i$

$X_{+i}$  = the marginal totals of column  $i$

$N$  = the total number of observations (Bishop, Feinberg, and Holland 1975).

**Table 4.3:** Accuracy assessment of water quality

Input Data	Acc(%)	Ua (%)	Pa (%)	K <sup>^</sup>
TM ,April 1986	95.1717%	93.267%	90.829%	0.49
TM ,October 1987	97.197%	93.426%	92.4604 %	0.94
ETM <sup>+</sup> April 2000	98.9973 %	97.179%	92.804%	0.97
ETM <sup>+</sup> December 2000	99.126%	97.179%	97.292%	0.98
OLI , April 2017	99.691%	99.263%	96.523%	0.99
OLI ,December 2017	99.2083%	99.016%	97.670%	0.98

According to gain results as clarified in table 4-3 which evaluate the performance accuracy for the MWQ section regarded to classification process for water quality as shown in figure 4-3 which described three categories of water for MDR with varying percentages of the area covered by each category for proposed input years and according to confusion matrix measures [1]. Thus, overall accuracy (Ac) evaluates pixels that classified properly [37] according to the diagonal elements of covariance matrix. Diagonal cells contain the number of correctly identified pixels. If we divide the sum of these pixels by the total number of pixels we will get classification's overall accuracy as expressed in equation (4.7).

Another accuracy indicator is the kappa coefficient (K<sup>^</sup>) as clarified in equation(4.10). It is a measure of how the classification results compare to values assigned by chance. It can take values from 0 to 1. If kappa coefficient equals to 0, there is no agreement between the classified image and the reference image. If kappa coefficient equals to 1, then the classified image and the ground truth image are totally identical. So, the higher the kappa coefficient, the more accurate the classification is[37][69].

Apart from the overall accuracy, the accuracy of class identification needs to be assessed. In order to do that, we have to look at non-diagonal cells in the matrix. These cells contain classification errors, i.e. cases when the reference image and the classified image don't match. There are two types of errors: underestimation (omission errors, omission) and overestimation (commission errors, commission).

For any class, errors of commission occur when a classification procedure assigns pixels to a certain class that in fact doesn't belong to it. Number of pixels mistakenly assigned to a class is

found in column cells of the class above and below the main diagonal. The amount of errors of commission is also described by the Producer's accuracy ( $P_a$ ) as clarified in equation (4.9).

In addition to, for any class, errors of omission occur when pixels that in fact belong to one class, are included into other classes. In the confusion matrix, the number of omitted pixels is found in the row cells to the left and to the right from the main diagonal. Thus, the amount of errors of omission is also described by the User's accuracy ( $U_a$ ) as clarified in equation (4.9)[69][70].



## 5. FEATURES EXTRACTION

RS has significant role in detecting and distinguishing the impact of climate changes on the earth surface. Most studies that recognize texture features extraction which leads to make use of statistical techniques to extract different features from input satellite images [36].

The objective of this chapter is to monitoring the changes of land cover which can be later used for wide variety of purpose. In addition to, extract the information that occurred in the areas which had affected with the variation of MDR water level space through period of 31 years, as well as the impact of climate changes which cause the degradation in areas and expansion the rest that located around the MDR through applying statistical calculations of DIP methods .

In this chapter further details will be given about combined classification algorithms regarded to unsupervised and supervised classification approaches those had been mentioned in chapter 4 through hybrid classification algorithm for detecting water quality section 4.2.5.1 .

### 5.1 LAND USE LAND COVER CLASSIFICATION (LULCC)

Through a period of years geomorphologic change in the LULC regions due to water body variations[86].Furthermore, Land cover information which can be acquired from RS data describes the spatial and spectral characteristics that reflect different cover types and lead to make distinguishing between covers related to the individual attribute for each cover type or features[87] .

Based on that, this section clarified and analyzed RS input temporal data for the years (1986-2017) as mentioned in table 1.2 to estimate the changes in LULC around the MDR to indicate its impact for different features over a period of time specifically after the degradation of water lake storage in recent years[88].

As illustrated in chapter 4, the classification process is the best approach for RS data to distinguish and identify different categories regarded to their signature reflectance, spectral and spatial information [80] as seen in section 4.2 that clarified water quality classes for MDR.

Furthermore, through classification a prior knowledge of all cover types is assumed and then used as base knowledge to identify the signature for each type which make the classification process more easier[19].

An important consideration in land cover classification is consistency and reproducibility. That is, the same result should be obtained by various analysts given the same input data or ideally, even different input data over the same area [87].

In general terms, clustering is an optimization problem that tries to find a partition of the data collection such that the items that belong to the same cluster are as similar as possible and the discovered clusters are as separate as possible based on a specified (dis)similarity metric within the high dimensional space that the data objects exist[89].

## **5.2 HYBRID APPROACH**

A hybrid approach is to use one of the automated classification methods to do an initial classification and then use manual methods to refine the classification and correct obvious errors. With this approach a reasonably good classification can be obtained quickly with the automated approach and then manual methods can be used to refine the classes(clusters) that did not get labeled correctly[80].

## **5.3 PROPOSED LAND COVER CLASSIFICATION ALGORITHMS (LULUC)**

In this section we clarified a performance for combining two methods which performed to detect land cover changes over years. Based on, clustering unsupervised and supervised k-means and SVM algorithms respectively to clarify hybrid LULCC approach to distinguish different types of land cover over years. In addition to, in this section the effectiveness of PCA approach has implemented to transforms the input data in such a way that indicated their similarity and differences for estimating land cover information. That is to say, it deals with the data through dimensionality reduction which refers to visualization of the data clearly and analyze it with more manageable[90] .This leads to optimal classification without any loss of information as possible as through hybrid process [91].

### **5.3.1 Features Selection /(PCA)**

Principal component analysis (PCA) is a statistical technique which widely used in RS for processing multispectral data. It is a multilateral technique that preserves much of relevant information through dimension reduction. Furthermore , its considered as unsupervised classification method[92][93].



Due to the objective of this chapter which related to distinguishing the patterns of LULC over years. This phase follow different context than previous chapter 4 in section(4.2.1) for observing the land cover information by hybrid classification through utilizing PCA approach to all visible and panchromatic bands to present the input data set for proposed Landsat's, to benefit the advantage of the individual property for each band under its electromagnetic wavelength[15].

The concept of PCA which was performed by Pearson in the year of 1991 for the first time is to move the set of input data sets of observation in which the variables may be correlated with each other into another sets of variables which are uncorrelated and called principal components. The mathematical procedure is finding an orthogonal matrix to transform the original data sets into another coordinate system where the principal components are located, such that the first principal component has the highest variance, and the second greatest variance which is orthogonal to the first and so on [94].

Consequently, the methodological process which has implemented in this phase as clarified in figure 5.3 introduces various DIP methods on the proposed data that mentioned in table 1.1 due to utilizing multiband data with different spatial resolution for performing PCA approach that leads unification their resolution for further processing[11].

Thus in ETM<sup>+</sup> and OLI has panchromatic band-8 with (15-meter) spatial resolution, so this indicated to applying pansharping method (PANS) to calibrate the spatial resolution for visible input multibands with panchromatic band. To do so, resampling process should being applied before implementing PANS it is necessary to undergo these data to correct location of pixels for different resolutions[95]. Thus, Nearest neighbor method has performed due to is consider simplest sampling method that used in remote sensing data which has property for keeping original values in the unaltered view [95]. Therefore, In this step generating of new pixel value was used by calculating the new pixel value in original image which was nearest to pixel value in new image (ROI), with keep the original image size during sampling.

Pan-sharpening method aims to include spatial information from a high-resolution image (high frequencies) into a low-resolution image (low frequencies) while preserving spectral properties of a low-resolution image[96]. After resampling the data, merging panchromatic image (band 8) with all other visible bands in order to enhance and increase their resolution through pan-sharpening process by proposed IHS (Intensity, Hue, and Saturation) analogy method which is sometimes permutated to HSI in the most literature. It was proposed by Siddiqui Yusuf in 2003.

This method has a vast improvement over traditional IHS for fusing satellite imagery that differs noticeably in spectral response. It allows combining single band PAN data with multispectral data, resulting in an output images with both clear and identified details [92] [97] . A histogram matching then had applied between new pan sharpening images(bands) and the original bands this allowed to obtain the distribution averages of intensity for the features between the Pan histogram and the reference histogram related to original data[98].

PCA is a linear dimensionality reduction technique which searches for projection in the maximum variability directions [104]. It computes the eigenvalues and eigenvectors of the data located in the covariance matrix. Since the covariance matrix of a set of centered or uncentred variables is the same, but it has the advantage of providing a direct connection to an alternative and more geometric approach to PCA [94]. Eigen vectors are sorted eigenvalues and the actual data is projected into the eigenvectors directions to center and scale the data. PCA will first standardize the extracted images after pan-sharpening process, and then the sample mean vector and standard deviation vector are calculated. Standardization of data means subtracting the sample mean from each observation, and dividing the product by the sample standard deviation. For an N dimensional image sample, the covariance matrix C of order NxN calculated as following equation (5.1)[91].

$$E = \frac{1}{N} \{(X - X^-)(X - X^-)^T\} \quad (5.1)$$

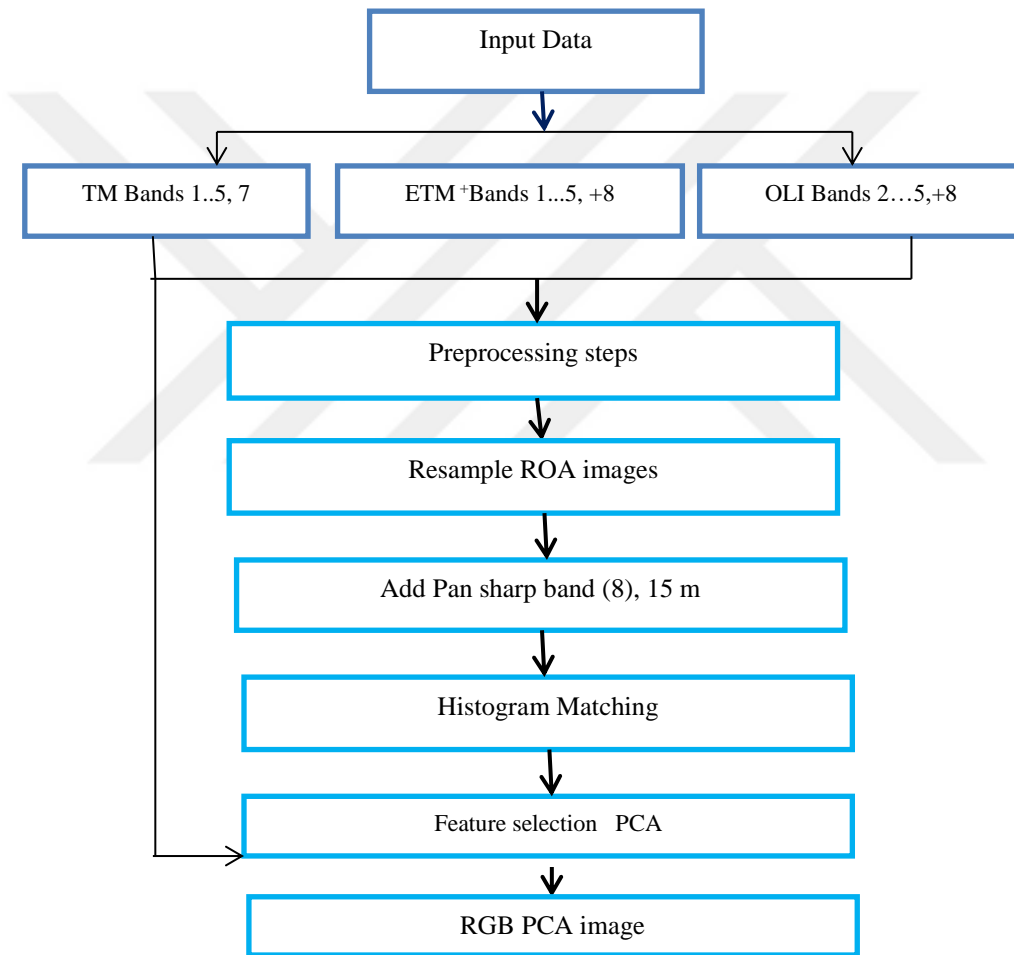
Where, X is the given matrix with NxN dimension and X<sup>-</sup> its mean vector. Then extract the Eigenvalues of C with the identity matrix (I) that defined by the following equation(5.2) which described the characteristics polynomial equation of matrix C with n roots [90].

$$Determinenet (C - \lambda I) = |(C - \lambda I)| = 0 \quad (5.2)$$

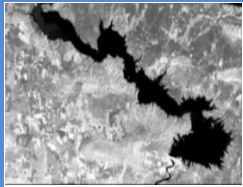
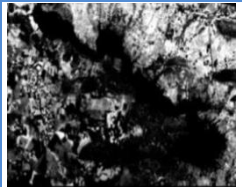
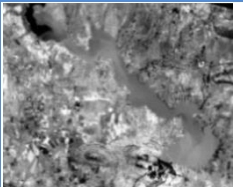
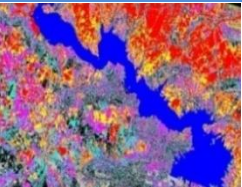
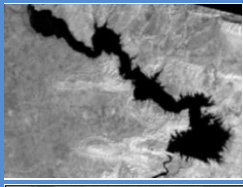
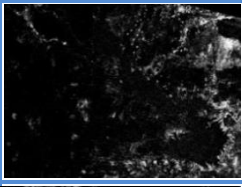
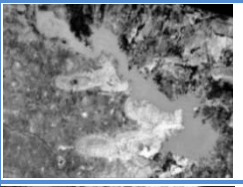
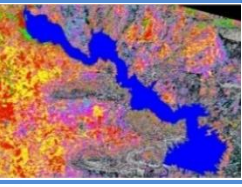

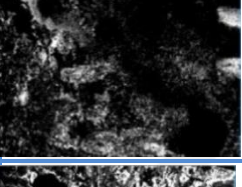

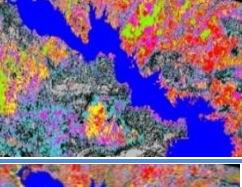
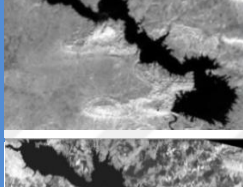
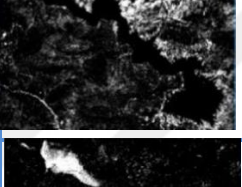
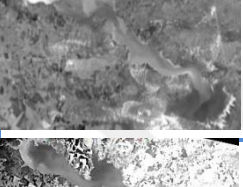
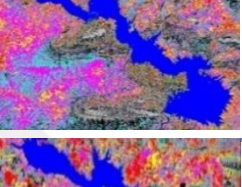
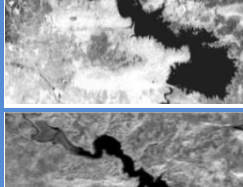
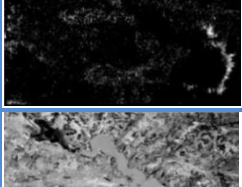
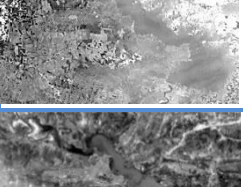
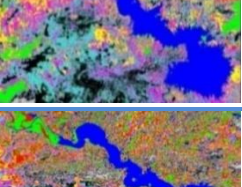
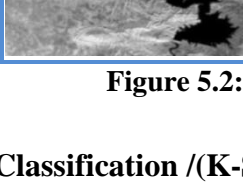
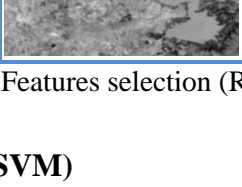
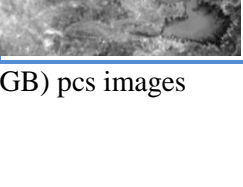
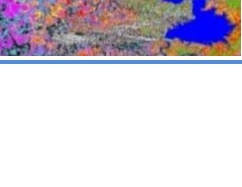
Furthermore , there were set of coordinates that correlated with each eigenvalue and defined the direction of the related principle axis which is called eigenvectors(x) as described in the following equation(5.3)[90].

$$Cx = \lambda x \quad (5.3)$$

After computing eigenvectors and sort eigenvalues in descending order, data is projected in the direction of the sorted eigenvector [22]. Noticed that , the dimensionality reduction for the projected data that extracted from PCA leads to visualization of the proposed data set with more clearly and analysis of the any number of input data set which resulting to three principle components image that displayed as color composite (RGB) image which is being more flexible to subsequent an optimal feature selection for hybrid clustering approach as shown in figure 5.4[93] .



**Figure 5.1:** Flowchart for PCA processing

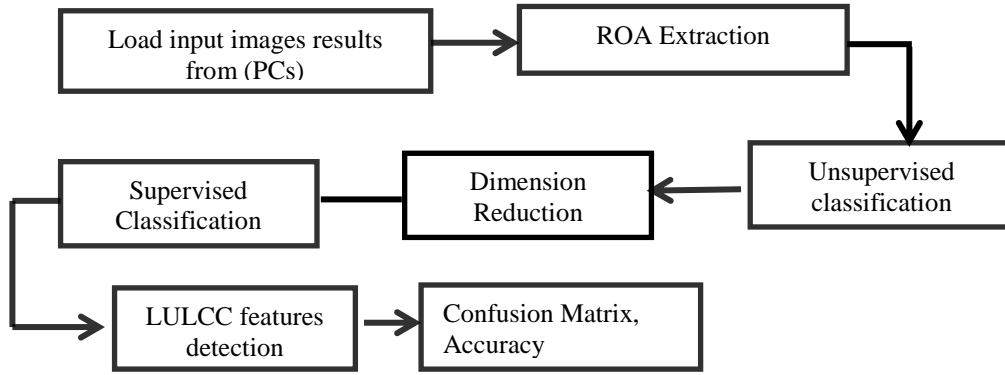
Captured date for input data	PC1	PC2	PC3	PCs(RGB) images
1986 , TM				
1987, TM				
2000/4 ETM <sup>+</sup>				
2000/12 ETM <sup>+</sup>				
2017/4 OLI				
2017/12 OLI				

**Figure 5.2:** Features selection (RGB) pcs images

### 5.3.2 Features Classification /(K-SVM)

A hybrid clustering algorithm is proposed by [99] which maximizes the common information between the clusters of multiple data types based on representation of the interaction between each pair of data types .

This section clarified the integration of unsupervised and supervised algorithms as clarified in figure 5.1 that represented by K-means and SVM sequentially to implement hybrid K-SVM process as clarified in chapter 4 specifically section 4.2.1 Furthermore, in this part includes extensive details about hybrid process which applied for LULCC extraction areas that located around the MDR as shown in figure 5-3.



**Figure 5.3:** Hybrid classification Process

Furthermore, in this phase we illustrated the property of PCA which based on data reduction. Thus, through the out images that extracted in section 5.3.1, clarified the PCA dimension reduction to perform data clustering according to K means objective function as clarified in equation 5.3[93] .

According to that, the RGB images that extracted from PCs implemented to give an initial set of k mean by  $k= 8$  data categories ,  $x_1, x_2, \dots, x_k$  , where  $\forall x_i \in R^w$  . In other word each  $x_i$  is normalized to be  $\| x_i \| = 1$ , and  $w$  represent the feature space. That is to say, K-Means partitions the  $x_i$  into  $k$  disjoint clusters  $\pi_1, \pi_2, \dots, \pi_k$ , [89] so that,

$$\bigcup_i^k \pi_i = 1 \text{ } \pi_i = \{x_1, x_2, \dots, x_n\} \text{ where } \pi_i \cap \pi_j = \emptyset \text{ } i \neq j \quad (5.4)$$

According to that each cluster  $\pi_i$  has the centroid  $c_i$  which clarified as equation 5.2, [89],[81]

$$C_i = \frac{\sum_{x^k \in \pi_i} X_j}{\|\sum_{x^j \in \pi_i} X_j\|} \quad (5.5)$$

In order to assign the features to their own clusters it should maximize the similarity between them. To do so, the objective function is needed between clusters that defined as in equation 5.3[89].

$$Max Q = \sum_{j=1}^k \sum_{x_i \in \pi_j} X_i^T \cdot C_j \quad \forall \pi_i \text{ } 1 \leq i \leq K \quad (5.6)$$

Noticed that K-means algorithm integrated with the prior view of features in field of study area and input image data[80] which utilized in this section to candidate eight clusters to identify different features that were located around the lake . However, the geomorphology of our region of study (ROI) noticed that various types of features in land cover acquired same spectral response which affected on the k-means clustering process. Thus, centers of some clusters will be more complicated to defined correctly [80] .

Based on that , SVM is needed here for controlling the complexity of k- means clustering results to gain accurate classifying data due to its attractively for processing RS data through finding the optimal hyperplane to distinguish between classes[35].Whereas, through RS classification specifically LULCC we should extract features clusters that they are identical with those in the base images and the geomorphological map of the study area[87].

Consequently, the K-SVM hybrid process clarified in this section through combining the out clusters from unsupervised k-means to be a train data for supervised SVM classifier process regarded to its ability to deal with high dimensional data that be suitable for classification process[82] and its efficiency to correct the out results of k-means by applying the regularization process [100] .After preparing all input images in preprocessing steps as clarified in section 4.2.1, this section clarified the hybrid process for all input data to extract LULC changing as displayed in figure 5.2. Here we will give extent details about the hybrid processing (K-SVM).

Noticed that the number of proposed categories (k=8) had taken after several experiments on the enhancements color images(ROI) to obtain a prior classified image that include most of the changeable features arbitrary by using ERDAS 9.1 software. To do so , the number of distinguished classes(8) being the initial input (k=8) in k-means process then the out (8)classes from k-means considered as input training data for SVM which concentrated for finding the optimal hyperplane to separate between classes through considering binary classification case by  $(x_i, y_i)$ ,  $i = 1, 2, \dots, N$  and  $y_i \in (-1, +1)$  ,where  $N$  is the number of training samples,  $y_i = +1$  for class  $\omega_1$  and  $y_i = -1$  for class  $\omega_2$  in case of we have two classes and linearly separable , as expressed in the following equation 5.4[42][89].

$$f(x) = w \cdot x + w_0 \quad (5.7)$$

According to that expression finding the optimal hyperplane for two classes ( $\omega_1, \omega_2$ ) respectively will be when both values  $w$  and  $w_0$  are evaluated in such a way that expressed the margin  $\frac{2}{\|w\|}$  and the optimal hyperplane then founded by  $\frac{1}{2} \|w\|^2$  [42] and defined as:

$$y_i (w \cdot x_i + w_0) - 1 \geq 0 \quad , i=0, 1, \dots, N \quad (5.8)$$

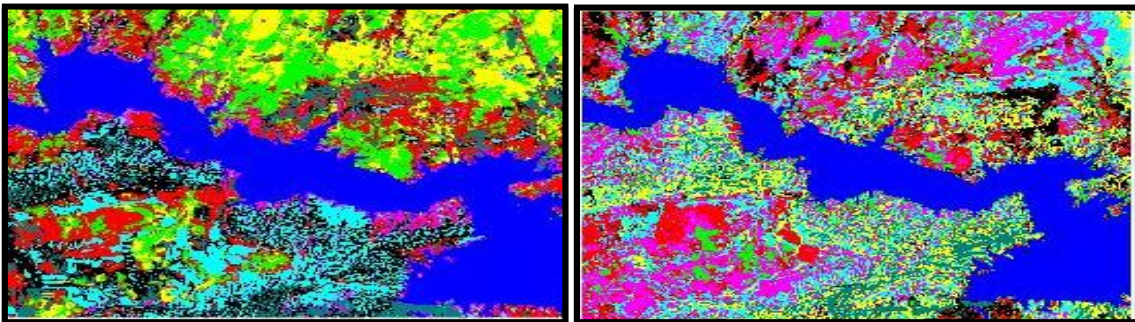
In our case we have more than two classes, so we need for classify SVM multi classes approach. Thus, the 8 classes had been extracted from k-means are being the training samples  $S$  in SVM space. Based on that, one against all process had implemented to separate the classes.

**One Against All** , all the training input data  $(x_1, y_1) \dots (x_k, y_k)$  where  $x_i \in \mathbb{R}^n$  ,  $i= 1 \dots k$ , and  $y_i \in \{1, \dots, N\}$  which is the class of  $x_i$  .Where is the  $i^{th}$  class in SVM trained samples will be positive (+1) and all other samples be negative(-1)[101]. Through this approach the classes had been not linearly separable and which is need to maximize the margin between the classes and minimize the error for most classes that had similar signature[104]. To do so, set of values added to equation (5.4) as the following equations (5.6) and (5.7) [42].

$$J = (w, w_0, \varepsilon) = \frac{1}{2} \|w\|^2 + C \sum_{i=1}^N \varepsilon_i \quad (5.9)$$

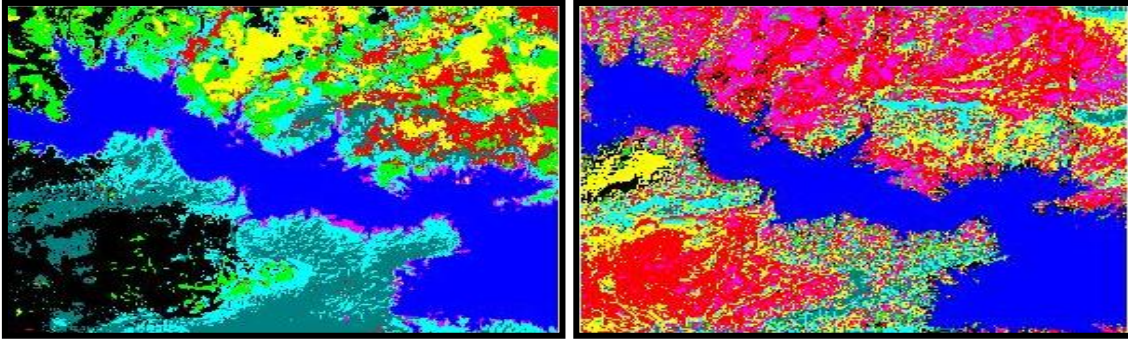
$$y_i (w \cdot x + w_0) \geq 1 - \varepsilon_i \quad (5.10)$$

Consequently, with this approach we can control and extract all features that identified as bad classes through k-means and consider them as classes in SVM training data , this is indicate to an essential impact about hybrid approach with multi-SVM related to reduce the dimension of the considering training data into binary processing [42].

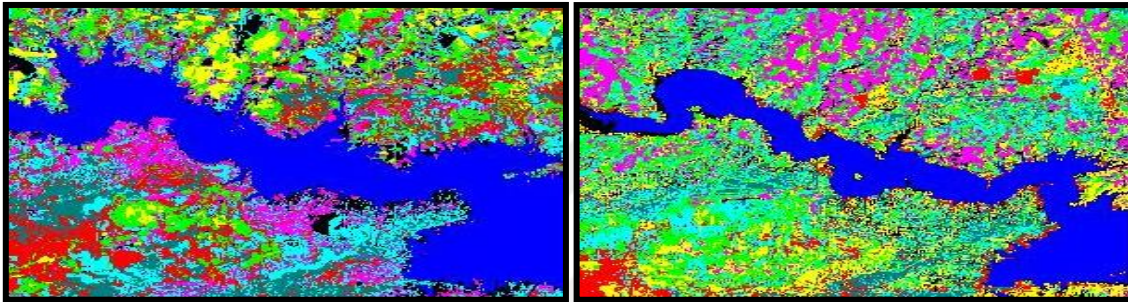


**Figure 5.4:** Hybrid classification process for TM of 1986 and 1987 years













**Figure 5.5:** Hybrid classification process for ETM<sup>+</sup> of 2000/Apr and 2000/Dec years



**Figure 5.6:** Hybrid classification approach for OLI data for the year 2017/Apr,2017/Dec

Hybrid Classification results as clarified in figures 5-4,5-5 and 5-6 are distinguish the variation of features for the input data of Landsat's TM, ETM<sup>+</sup> and OLI respectively. Such as two seasons were proposed to detect the impact of climate changes in rainfall season which represented winter for the input data of the years 1987/October, 2000/December and 2017/December that clarified the classification images result in the right hand side, and spring season for the input data of the years 1986/April, 2000/April, and 2017/April that seen in the left hand side of figures 5-4, 5-5 and 5-6. Out results of the classification extracted different features around MDR represented with different eight classes as clarified in table 5.1.

**Table 5.1:** Classes Identification and areas

Class Number	Class Type
Class-1 	Mosul Dam's Lake
Class-2 	Vegetation
Class-3 	Slope Deposits and Soil
Class-4 	Accumulation Classic
Class-5 	Erosional terraces and recent deposits
Class-6 	Outcrops
Class-7 	Valley filling Deposits
Class-8 	Residual Soil



Whereas, each indicated class (feature) has different color which it identified with in the land cover area around reservoir. Such as class1 has blue color to identify MDR, class 2 with green color reflect the vegetation areas, and so on, as clarified in figures 5.4, 5.5 and 5.6 respectively. Furthermore, there is a significant variation in covered areas for each category over years and proposed seasons as well; this is due to different environmental impacts [5]. Such as ,each class(feature) has different area rate over years as will clarified in next section that related to features extraction performance.

## **5.4 PERFORMANCE ACCURACY (AC)**

### **5.4.1 PCA Performance**

As clarified in section 5.3.1 PCA is a powerful method for analyzing data[94]. In order to get optimal analyzing through PCA work properly, the first step we have to subtract the mean for each of the input data dimensions to produce a data set whose mean is zero and all variables will transformed to same scale in case there were large differences in their scale [104].

Next significant step is calculating covariance matrix in order to understand how the variables of the input data set are varying from the mean with respect to each other, or in other words, to see if there is any relationship between them. Because sometimes, variables are highly correlated in such a way that they contain redundant information [69]. Then from this matrix we need to compute two linear algebra concepts represented by finding Eigen values and their corresponding Eigenvectors matrix as calculated through MATLAB regarding to equations (5.2) and (5.3) which are demonstrated above.

That is to say, applying Eigenvectors matrix provide a significant justification of PCA based on data reduction which performs good guided for Means centers through clustering process [93], and the largest variances which represented with Eigen values will be the first principle component account [94].

Based on that, tables form 5.2-5. , clarified Eigenvectors matrix that extracted from covariance matrix for the TM Landsat PCs images (bands) Thus for each input band the output result for it represented with PC component , and for the year 1986 we proposed six bands according to that the output will be six PCs components .

**Table 5.2:** Eigenvectors Matrix for TM data for the year 1986

PCs component Bands No:	PC1	PC2	PC3	PC4	PC5	PC6
Band1	0.298	-0.334	-0.310	0.586	-0.529	-0.279
Band2	0.235	-0.173	-0.220	-0.285	0.237	0.853
Band3	0.425	-0.258	-0.164	-0.014	0.739	-0.422
Band4	0.473	0.849	0.210	0.082	-0.040	-0.028
Band5	0.264	0.033	0.874	0.400	0.052	0.010
Band7	0.616	0.260	0.134	-0.638	-0.335	0.118

The significant objective from obtaining covariance matrix is Eigen vectors matrix, which specified the directions of the axes where the rich information with highest variance to decide the best PCs. whereas the first Pc has the biggest value of variance and the second has the next variance and so on [69].

As clarified in table 5-2 , the Eigenvectors matrix performed the data for TM Landsat for 1986 for 6 input data set.

The eigenvalues are the coefficients that correlated to eigenvectors. According to the above table we get 6 eigenvalues which were extracted from the eigenvectors matrix and present the Pcs.

Thus, ranking the eigenvectors matrix in the descending order related to their eigenvalues.

The eigenvalues ordered from highest to lowest order and obtain the PCs according to that order of significance.

In addition to, another input data set related to TM Landsat as clarified in table 5.3 which Calculating the covariance matrix for the data set the 1987 year. Based on that, eigenvectors matrix values extracted.

**Table 5.3:** Eigenvectors Matrix for TM data for the year 1987

PCs component Bands No:	PC1	PC2	PC3	PC4	PC5	PC6
Band1	0.251	-0.243	0.135	-0.182	-0.330	0.121
Band2	0.310	-0.241	-0.240	0.066	0.032	-0.021
Band3	0.248	0.132	-0.122	-0.871	-0.298	0.541
Band4	0.520	-0.047	0.751	-0.542	0.125	-0.314
Band5	0.426	-0.266	-0.162	0.781	-0.534	0.100
Band7	0.510	0.012	-0.891	-0.253	0.119	-0.431

According to the direction of transformation as clarified in equation (5.3) noticed two types of extracted values (positive and negative) in the eigenvectors matrix this due to the situation when  $\lambda < 0$ , and so the vector points being in the opposite direction but still on same line[104] . According to that, the corresponding scalar eigenvalues affect in this transformation as well as [69].

**Table 5.4:** Eigenvectors Matrix for ETM<sup>+</sup> data for the year 2000/April

PCs component Bands No:	PC1	PC2	PC3	PC4	PC5	PC6
Band1	0.128	-0.511	0.374	-0.597	-0.129	-0.456
Band2	0.206	-0.489	0.248	-0.023	0.190	0.78
Band3	0.430	-0.432	-0.033	0.708	0.013	-0.353
Band4	0.274	0.452	0.760	0.178	0.325	0.053
Band5	0.624	0.324	-0.072	-0.249	0.652	-0.105
Band8	0.538	0.048	-0.461	0.215	-0.643	0.184

Noticed from eigenvectors matrix values for the data set of ETM Landsat for the year of 2000/April, has positive and negative values as well. Generally, eigenvector matrix applied negative eigenvalues whenever it  $Cx = -\lambda x$ , for some  $\lambda > 0$ , which can happen in a lot of ways in addition to in case of  $\lambda < 0$  [94] as clarified in table 5-2.

Furthermore, the eigenvectors matrix for the data set related to ETM<sup>+</sup> Landsat for the year of 2000/December as clarified in table 5-5.

**Table 5.5:** Eigenvectors Matrix for ETM<sup>+</sup> data for the year 2000/December

PCs component Bands No:	PC1	PC2	PC3	PC4	PC5	PC6
Band1	0.137	0.548	0.205	0.685	0.411	0.220
Band2	0.541	0.116	0.532	0.553	0.320	0.269
Band3	0.235	0.205	0.402	0.173	0.842	0.834
Band4	0.278	0.636	0.643	0.291	0.134	0.014
Band5	0.744	0.488	0.312	0.330	0.008	0.152
Band8	0.485	0.121	0.835	0.218	0.043	0.526

Consequently, the table clarified a matrix with positive values which perform positive eigenvalues as well. That is to say, this due to that all elements for the covariance matrix (C) are real and nonnegative. In other words  $C \geq 0$  and for some  $\lambda > 0$  [94].

**Table 5.6:** Eigenvectors Matrix for OLI data for the year 2017/April

PCs component Bands No:	PC1	PC2	PC3	PC4	PC5	PC6
Band1	0.125	0.492	0.076	0.415	0.304	0.047
Band2	0.643	0.149	-0.500	0.038	0.360	0.464
Band3	0.237	0.749	0.215	0.430	0.006	0.053
Band4	0.175	0.725	0.1501	0.322	0.389	0.168
Band5	0.647	0.205	0.504	0.011	0.543	0.197
Band8	0.334	0.120	0.475	0.034	0.014	0.328

Noticed in table 5-6 , the entries of eigenvectors matrix has one negative value that is to say when we interpret the matrix geometrically, we can say that it has a negative value represents a linear transform which acts as a reflection across some axis. Furthermore, when the matrix is non-zero and negative semi-definite then it will have at least one negative eigenvalue [90].

For the input data set related to OLI Landsat for the year 2017/December, as demonstrated in table 5.7, which extract eigenvectors matrix values depending on the covariance matrix calculations[69].

**Table 5.7:** Eigenvectors Matrix for OLI data for the year 2017/December

PCs component Bands No:	PC1	PC2	PC3	PC4	PC5	PC6
Band1	0.357	0.392	0.447	0.498	-0.398	0.228
Band2	0.636	-0.022	-0.298	-0.398	0.750	-0.089
Band3	0.268	0.453	-0.126	0.190	0.002	0.671
Band4	0.626	0.282	0.069	-0.599	0.389	0.771
Band5	0.447	0.320	0.681	0.239	0.036	0.189
Band8	-0.89	0.582	0.475	0.034	0.014	-0.328

In the extracted table 5-7 it can clarified that the eigenvector matrix contain both positive and negative elements, this led to get at least negative Eigen values [90]. That is to say, a matrix is real and has more than negative values through its diagonal [94].

Based on the above, table 5-8 clarified elicitation of Eigenvalues for each Eigenvectors matrix

**Table 5.8:** Eigenvalues for all data set

PCs component Data set:	Eigv-pc1	Eigv-pc2	Eigv-pc3	Eigv-pc4	Eigv-pc5	Eigv-pc6
1986/April	0.9102	0.8886	0.8169	0.3844	0.3596	0.1998
1987/October	-0.0382	-0.0391	-0.0989	-0.2586	-0.4338	-1.086
2000/April	0.8739	0.8529	-0.3281	0.2771	-0.892	-0.9017
2000/December	0.7503	0.4544	0.3847	0.3933	0.2140	-1.2375
2017/April	1.0923	0.5434	0.2133	0.2960	0.1589	0.0831
2017/December	0.7018	0.6686	0.6321	-0.8772	0.4129	-0.2864

According to the Eigenvectors matrix as clarified in the above tables, table 5.8 demonstrated the Eigenvalues elements for each of the input data set , based on the values in Eigenvectors matrix. Consequently, the first PC will take the highest Eigenvalue which represent the highest variance [104], and second PC the second variance and son on.

As clarified in figure 5.2 the extracted image from feature selection process include the first three PCs according to their Eigenvalues elements. Thus the first three Pcs combined to extract one RGB image, whereas Pc1 represent the biggest Eigenvalue and the second Pc2 include the second value and so on[90].

#### **5.4.2 Features Extraction Performance -LULCC**

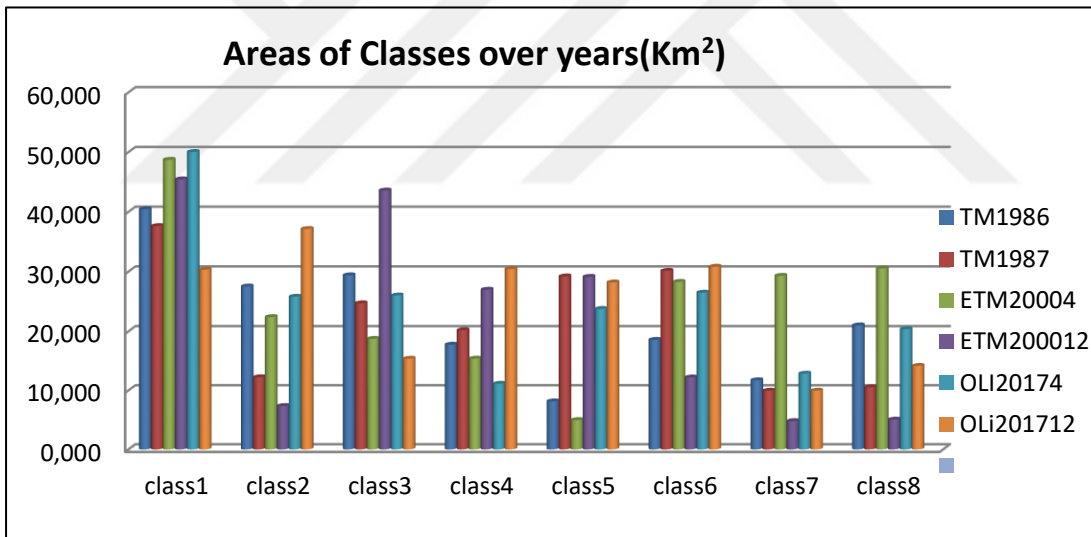
Accuracy assessment is one of the significant steps in Land use /Land cover classification (LULCC), due to its property to assess how the points (samples) are belong to the correct features in the land cover area effectively[85].

The aim of this section is to distinguish the differences between features that covered the area which located around Mosul dam using RS data from 1986-2017 years. In addition to, distinguish different types of features which are located around the MDR, and how the variation in its water level has affected the covered areas for each feature . Consequently, the hybrid classification process extracted 8- classes (categories) to identify the features of the specified study area which contained various categories. That is to say, table 5.7clarified the types of 8- categrioies (classes) that can be recognized around Mosul dam area. Furthermore, as demonstrated in chapter 4, section 4.3 the areas in (km<sup>2</sup>) of each class were calculated by the equations (4.5), and (4.6) respectively to detect the changes in each class over years, as clarified in table 5.8.

**Table 5.9:** Calculated area for classes over years

Input Data	Classes areas ((km <sup>2</sup> ))							
	Class1	Class2	Class3	Class4	Class5	Class6	Class7	Class8
TM ,1986	40.4397	27.5139	29.3895	17.7552	8.1496	18.5688	11.7207	21.005
TM ,1987	37.6335	12.2364	24.7095	20.1474	29.2086	30.1338	9.953	10.5201
ETM <sup>+</sup> ,2000/4	48.7206	22.3974	18.7425	15.39	4.979	28.2879	29.304	30.5325
ETM <sup>+</sup> ,2000/12	45.4446	7.3566	43.5789	26.9721	29.1249	12.2031	4.8042	5.058
OLI ,2017/4	50.0328	25.8003	26.0118	11.1294	23.7627	26.4789	12.8412	20.3598
OLI ,2017/12	30.339	37.1391	15.3747	30.4308	28.1961	30.8223	9.9621	14.1525

Obviously, to estimate the actual variation of the land cover features represented with the extracted 8- classes which were located around the lake of Mosul Dam , figure 5.5 demonstrated the statistic graph of the above table 5.8. In addition to, figures 5.6, and 5.7 clarified the graph of the calculated area of each class regarded to the years of input data.



**Figure 5.7:** Estimated graph for distinguishing the areas over years

Another approach for measuring the performance accuracy assessment is a vital and an important part in any classification process, whether used technique is supervised or unsupervised classification, is an assessment of the accuracy of the generated image classification. The most common way used to assess the accuracy of classified image is to create random points of ground truth and compare the classified data in a confusion matrix. Thus, due to our lack of accessed for a ground truth for all of data that used in this study , therefore we had used same images(input data) to create basic classification for ROI images In order to properly generate an error matrix which is based on pixel by pixel between the reference data and the basic classification that we

implemented . Such matrixes are square, with the number of rows and column equal to the number of the categories whose classification is being assessed evaluating the references coefficient[46]. The overall accuracy of classification compares how each pixels of classified image is classified against the definite land-cover obtained from their corresponding ground truth data. Overall accuracy computed by dividing the total correctly classified pixel by the total number of reference pixels in the error matrix.

The producer’s accuracy is calculated by dividing the total number of the correct pixels in a category by the total number of pixels of the category that derived from, and this descriptive statistic compute the accuracy of individual categories [82]. While the user’s accuracy is calculated by dividing the total number of correct pixels in a category by the total number of pixels that were actually classified in that category, and this indicator determine the probability that a pixel classified on the image actually represents that category on the ground. Finally, the Kappa coefficient is a quantitative assessment of the error matrix, and it is a measure of the difference between the observed agreement between two maps and the agreement that might be attained solely by chance matching of the two maps[102].

Consequently, hybrid classification performance for LULC is a significant approach that demonstrate the assessment accuracy of land cover classification for remote sensing data properly[70][84]. Based on, applying an error matrix (confusion matrix) as demonstrated in chapter 4, section 4.3 regarded on calculating the overall accuracy (Acc), Producer accuracy(Pa), Users accuracy(Ua) and Kappa coefficients( $K^{\wedge}$ ) . Regarded to equations (4.7, 4.8, 4.9 and 4.10), as shown in table 5.9.

**Table 5.10:** Assessment accuracy for classification approach

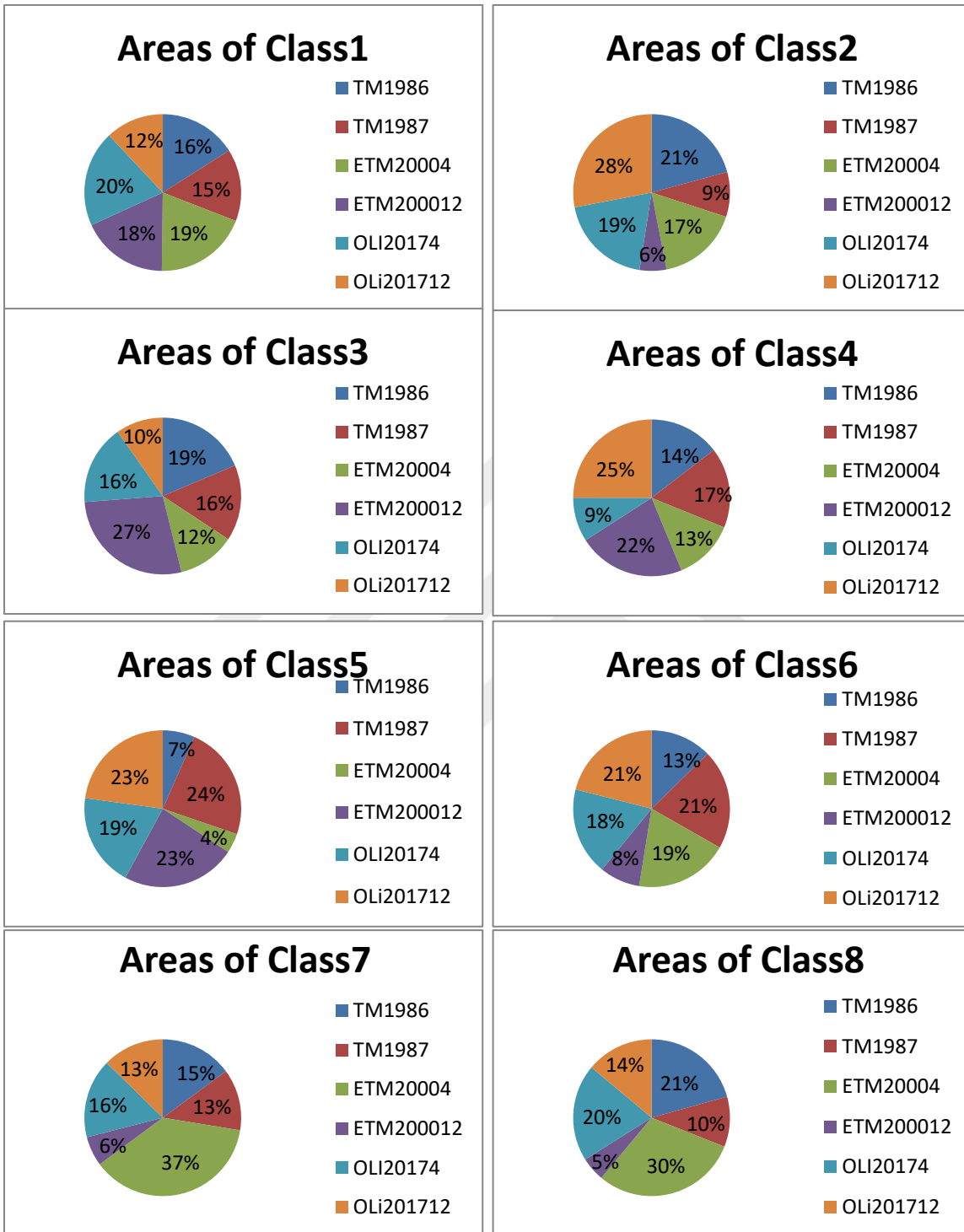
Used Data set	Overall Accuracy(Ac)%	Producer Accuracy(Pa)%	Users Accuracy(Ua)%	Kappa ( $K^{\wedge}$ )%
TM ,1986	93.809	90.075	92.362	92.751
TM ,1987	94.883	92.248	92.018	93.970
ETM+ 2000/4	97.179	95.751	96.854	96.695
ETM+ 2000/12,	97.019	96.180	96.061	96.265
OLI ,2017/4	98.514	98.55	98.418	98.243
OLI ,2017/12	98.870	98.335	97.185	98.126

Obviously, table 5.10, clarified the performance of LULCC process by utilizing hybrid classification which described eight categories of different land cover features that located around MDR. Thus, overall accuracy (Acc) evaluates pixels that classified properly [37] according to the diagonal elements of covariance matrix. Diagonal cells contain the number of correctly identified pixels. If we divide the sum of these pixels by the total number of pixels we will get classification's high performance through overall accuracy as expressed in equation (4.7) ,chapter 4. In addition to , the performance evaluated with another criteria's as clarified in table 5.9. Another accuracy indicator is the kappa coefficient ( $K^{\wedge}$ )as clarified in equation(4.10). It is a measure of how the classification results compare to values assigned by chance. It can take values from 0 to 1. Such as, in case kappa coefficient equals to 0, there is no agreement between the classified image and the reference image. If kappa coefficient equals to 1, then the classified image and the ground truth image are totally identical. So, the higher the kappa coefficient, the more accurate the classification is[37][69].

Apart from the overall accuracy, the accuracy of class identification needs to be assessed. The amount of errors of commission is also described by the Producer's accuracy (Pa) as clarified in equation (4.9). In addition to, for any class, errors of omission occur when pixels that in fact belong to one class, are included into other classes. In the confusion matrix, the number of omitted pixels is found in the row cells to the left and to the right from the main diagonal. Thus, the amount of errors of omission is also described by the User's accuracy(Ua) as clarified in equation (4.9)[69][70].

In order to obtain more accurate results, figure 5.8 clarified another type for evaluating the performance of LULCC approach by applying statistical graph to demonstrate the distribution of areas for each class over the years of input data set.



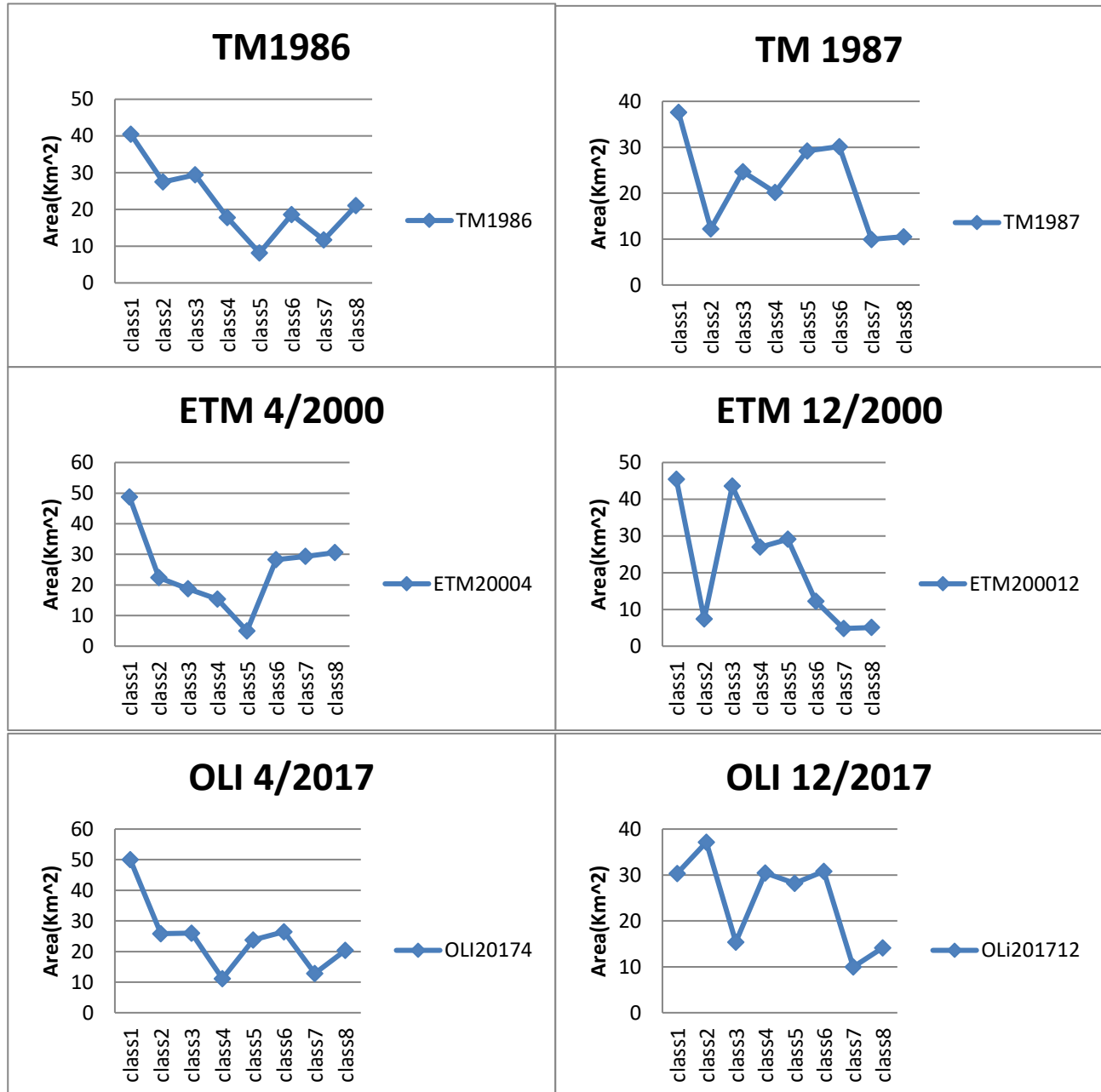


**Figure 5.8:** Distribution areas for each class over years

According to the classes that extracted from the classification process as clarified in table 5.8, figure 5.8 demonstrated the distribution for each feature (class) over the input data sets. That is to say, the graph confirms that the impact of climate changes over years. Thus, class 1 that reflect the blue color as illustrated in table 5.1 and identified MDR feature which has covered area with maximum percentage

value in the year of 2017/April and minimum covered area in the year of 2017/December ,as clarified in **Areas of class 1** of figure 5.8 based on the percentage values graph for all implemented years. And so on for the other classes that occupied different space areas related to the variation of land cover that happened over years of period due to environmental changes[94].

As confirmation for the above, figure 5.9 clarified another side for classes distribution graph based on proposed input data set.



**Figure 5.9:** Distribution classes areas for each proposed year

As clarified in the above graph of figure 5.9 which reflected the amount of covered areas for the extracted classes over each proposed data set . Thus, it noticed that the classes had Oscillating curve which based on their amount values for the areas that they identify the features. Such as, its obvious from the curve the sequence of covered areas for each category per kilometers as demonstrated in table 5.8 and figure 5.7 for the proposed input data set. For instance , in the year of 1986 class 1 represented with MDR exploits maximum area reach to(40 KM<sup>2</sup>) comparing with other classes , while class 2(vegetation) occupied (21 KM<sup>2</sup>) , and so on.

However, its clear to evaluate the differences of covered areas for the same class between suggested years due to the season period and the input year [94].



## 6. CONCLUSIONS AND FUTURE WORK

This study shows, evaluating the effect of climate changes over different years based on three main temporal remote sensing Landsat's data combined with various digital image processing techniques through MATLAB environment which improved its efficiency as suitable tool for monitoring water resources.

In order to achieve the objective goal for this study, we proposed different algorithms based on choosing Mosul Dam's lack as study area location due to the significance of this area related to its water source storage that entered from Tigris river as well as the receding of its water storage level that noticed in last years and its water quality as well due to climate and environmental factors over different years. This chapter will include two phases, first demonstration of gained results and second conclusions of implemented study.

### 6.1 ANALYSIS OF RESULTS

Current study utilized MATLAB2015 version software under operating system with an (Intel), 8 GB Ram, 2.40 GHz and Windows 10, to implement the processing for desired temporal satellite data for different Landsat's that is acquired from Landsat-5 TM, Landsat-7 ETM+ and Landsat-8 OLI over periods of years , were utilized as input data which is listed in table 1.1 to estimate and monitor the environmental changes that occurred in the areas that covered with water surfaces over period years by performing a set of DIP sequential steps .

The extracted results improved the compatibility of Matlab software are remote sensing data and image processing applications. We applied temporal remote sensing data for implementing the methodology of this work as displayed in figure 3-2, so they needed to geometric correction as the first step from preprocessing for all sections that implemented in this work , in order to collect more information that is reflected from more wavelength ranges[23] which avails the objective of this study.

Consequently, multi-bands combination method used to get one true color composite images that converted to gray one to be more easier through utilizing further processing [104]. It is worth mentioning, that we had used near -infrared as (Red) channel, shortwave infrared as (Green) channel for two Landsat's due to their abilities to distinguish between lands and water [103] thus, (Blue) channel represented with band-1 for ETM+ Landsat , and band-2 for OLI Landsat. Whereas, band-1 in various Landsat's represented with blue normal color which is suitable for

water studying due to its high reflectivity for the water through its wavelength[23] ,while in Landsat 8 (OLI) band-2 perform the same purpose regarding to the same wavelength of band-1 in ETM+ [11] . Therefore, we utilized combined bands (5,4,1) for ETM+ data and (5,4,2) for OLI data as clarified in figure 3-2.

### **6.1.1 Fundamental of Water Extraction Analysis**

The first phase of this work has a context for evaluating the water surfaces for various water surfaces that entered in Mosul city as seen in figure 1-1 which is described study area location.

Different methods proposed to implement the processing for desired temporal satellite data that is acquired from Landsat-8 (OLI) in 2015 and Landsat-7 (ETM+) in 2002, were utilized as input data which is listed in Table 1-1, to estimate and monitor the environmental changes that occurred in the areas that covered with water surfaces over period of 13 years.

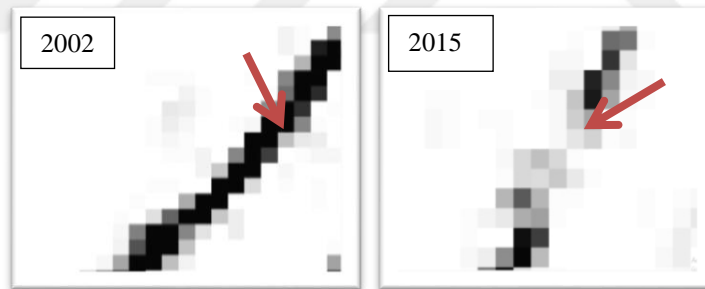
The extracted results improved the compatibility of Matlab software remote sensing data and image processing applications through applying temporal remote sensing data for implementing the methodology of this section. Figure 3-7, clarified the results of post-processing for evaluating the differences between water surface areas in Mosul city over 13 years period by utilizing two input data related to ETM<sup>+</sup> of the year 2002 and OLI of the year 2015 by considering threshold value to obtain binary image from gray one as simple step to isolate whole water surface areas, then implementing morphological operations with structuring elements using kernel(5x5) to detect the exact shape and boundary of extracted object areas , due to having different shapes of areas that are covered with water. Finally, to get rid of any ambiguous pixels, remove noise median filter was used trying to obtain the out shapes of water surface areas without mixing pixels that belong to other features (non-water).

The results clarify various measurements of segmented areas that are occupied by water bodies which represented with Tigris river, Mosul Dam reservoir, and small swamps from input data to evaluate the performance of proposed methodology, by calculating the number of pixels for segmented water objects surfaces regarding the suggested threshold value. Consequently, the segmented areas of water surface from ETM+ in the year 2002 has covered (240384) number of pixels, while the areas that covered with water bodies from OLI in 2015 has covered (223485) number of pixels according to the intensity of water that recorded values less than threshold

which acquired the segmented area by pixels. Based on this information, a spatial resolution of input satellite images for each pixel was equalized to 30 meters, (30x30) which means each pixel on satellite images represented by the square 30 m<sup>2</sup> in the field location[7][72] .

In addition to, there another performance demonstrated in this phase to evaluate the obtained results by calculating the accuracy based on segmented objects which indicated the performance of extracted whole areas that are covered with water to the whole pixels in an image. Thus, table 3-2 described performance accuracy for the extracted results and figure 3-7 clarified water surfaces represented with Tigris river, Mosul Dam reservoir and small swamps were all recognized in 2002 year.

In other words, we can conclude the results in the year of 2015 the are small swamps became dried, and in the northeast of Tigris river there were places exhausted from the water comparing with same area in the year of 2002 this side was full of water, in order to obtain guarantee about that we zoomed a clip part from the resulting images as shown below:



**Figure 6.1:** Clip part shows water surface receding

This difference of water shape illustrated that there were many misleading pixels that belonged to water surface area of Tigris River in the year of 2002, while in the years of 2015, they have been contaminated or dried which indicated decreasing of the accuracy value in the year of 2015 as clarified in table 3-2.

### **6.1.2 Analyze the Evaluation of Water State Results**

According to gain results as clarified in table 4-3 which evaluate the performance accuracy for the MWQ section regarded to classification process for water quality as shown in figure 4-3 which described three categories of water for MDR with varying percentages of the area covered

by each category for proposed input years and according to confusion matrix measures [1]. Thus, overall accuracy (Acc) evaluates pixels that classified properly [37] according to the diagonal elements of covariance matrix. Diagonal cells contain the number of correctly identified pixels. If we divide the sum of these pixels by the total number of pixels we will get classification's overall accuracy as expressed in equation (4.7).

Another accuracy indicator is the kappa coefficient ( $K^{\wedge}$ ) as clarified in equation (4.10). It is a measure of how the classification results compare to values assigned by chance. It can take values from 0 to 1. If kappa coefficient equals to 0, there is no agreement between the classified image and the reference image. If kappa coefficient equals to 1, then the classified image and the ground truth image are totally identical. So, the higher the kappa coefficient, the more accurate the classification is. [37][69]

Apart from the overall accuracy, the accuracy of class identification needs to be assessed. In order to do that, we have to look at non-diagonal cells in the matrix. These cells contain classification errors, i.e. cases when the reference image and the classified image don't match. There are two types of errors: underestimation (omission errors, omission) and overestimation (commission errors, commission).

For any class, errors of commission occur when a classification procedure assigns pixels to a certain class that in fact doesn't belong to it. Number of pixels mistakenly assigned to a class is found in column cells of the class above and below the main diagonal. The amount of errors of commission is also described by the Producer's accuracy ( $P_a$ ) as clarified in equation (4.9).

In addition to, for any class, errors of omission occur when pixels that in fact belong to one class, are included into other classes. In the confusion matrix, the number of omitted pixels is found in the row cells to the left and to the right from the main diagonal. Thus, the amount of errors of omission is also described by the User's accuracy ( $U_a$ ) as clarified in equation (4.9)[69][70].

### **6.1.3 Features Extraction Analysis**

The objective of this section is to distinguish the differences between features that covered the area which located around Mosul dam using RS data from 1986-2017 years. In addition to, how the variation in its water level has affected the covered areas for each feature. Consequently, the hybrid classification process extracted 8- classes (categories) to identify the features of the specified study area which contained various categories. That is to say, table 5.8 clarified the

types of 8-categories (classes) that can be recognized around Mosul dam area. Furthermore, as demonstrated in chapter 4, section 4.3 the areas in (km<sup>2</sup>) of each class were calculated by the equations (4.5), and (4.6) respectively to detect the changes in each class over years, as clarified in table 5.8.

To evaluate the performance of method that implemented to extract the actual variation of the land cover features represented with the extracted 8- classes which were located around the lake of Mosul Dam , figure 5.5 demonstrated the statistic graph for the classes area as clarified in table 5.8. In addition to, figures 5.6, and 5.7 clarified the graph of the calculated area of each class regarded to the years of input data in order to confirm the differences in land cover over years.

## **6.2 CONCLUSIONS**

To conclude this work, we emphasize that the temporal remote sensing data has a significant impact to evaluate the changes in the water state through a spectral and spatial resolution for various satellites data. Due to, environment and climate changes, two types of Landsat images were examined in this study in cooperation with digital image processing techniques had implemented to evaluate and analyzed the water state over years due to climate changes and decreasing the average of rainfall in its seasons. The output result images and calculations demonstrate the weather changes over the years on the most significant feature of the land cover which is represented with water. Thus, through this work, the changes of different water surfaces had observed temporarily in Mosul city. Such as, the extracted results improved receding of water surface over (13) year's period. In other words, the results and calculations illustrate the total areas covered with water in Mosul city noticed decreasing of their surface in the year of 2015, in addition to, draught of small meres That leads to confirm the fact that the lack of rainwater in recent 13 years during the rainfall seasons with increasing temperature over the average in summer, not just in Mosul city but whole Iraq which led to decreasing area and level of water surface.

According to the extracted results, we can conclude the proposed methodology has the advantage to extract the water surface areas with different shapes and good accuracy. In addition to, remote sensing data have significant integration with different digital image processing techniques



which evaluate and interpret various issues related to detect or extract many types of objects (features) from satellite data which can be benefit for different fields of studies which are interested in land cover recognition. Furthermore, we can clarify the efficiency of the MATLAB program and its toolbox library to process temporal remote sensing data in spite of the big size of all input data with less execution time and gain clear and accurate results with high accuracy

### **6.3 FUTURE WORK**

Commenting on the above demonstrations, this thesis concentrate on utilizing combined digital image processing techniques and temporal remote sensing data to evaluate the impact of climate and environmental variations for the water surfaces and different land covers over specific period of years. Hybrid approach through classification process and different digital image processing methods approved their abilities to achieve the desired goal of this work.

Consequently, its motivating in future implements a simulation system to monitor changes across the water-covered areas in whole Iraq and not just in a specific area due to sudden climate changes in recent years by using temporal data with wide period .

Obviously, for coastline extraction three methods were utilized here, in future hybrid approach can be proposed to ensure obtaining high performance extraction. Furthermore, hybrid classification approach through unsupervised and supervised techniques is performed to extract water level, water quality and Land Cover classification .In future , deep learning technology characterized by different neural networks(NNs) approaches are utilized in remote sensing data classification for land use/ land cover areas (water/Land) .

## REFERENCES

- [1] C. J. Poortman, J. P. Saba, I. Andersen, V. Jagannathan, and A. S. M. A. Ghany, "Iraq - Country water resource assistance strategy: addressing major threats to people's livelihoods," no. 36297, pp. 1–97, 2006.
- [2] "City Profile of Mosul , Iraq," no. October, 2016.
- [3] A. S. Muhaimed, "Evaluation of long-term vegetation trends for northeastern of Iraq : Mosul , Kirkuk and Salah al-Din," vol. 5, no. 2, pp. 67–76, 2013.
- [4] M. F. O. Khattab, R. K. Abo, S. W. Al-Muqdadi, and B. J. Merkel, "Generate Reservoir Depths Mapping by Using Digital Elevation Model: A Case Study of Mosul Dam Lake, Northern Iraq," *Adv. Remote Sens.*, vol. 06, no. 03, pp. 161–174, 2017.
- [5] P. Ceccato and T. Dinku, "Introduction to Remote Sensing for Monitoring Rainfall , Temperature , Vegetation and Water Bodies," p. 15, 2010.
- [6] US Department of the Interior and US Geological Survey, "Spectral bands," pp. 1–2, 2013.
- [7] T. D. Acharya, D. H. Lee, I. T. Yang, and J. K. Lee, "Identification of water bodies in a landsat 8 OLI image using a J48 decision tree," *Sensors (Switzerland)*, vol. 16, no. 7, pp. 1–16, 2016.
- [8] D. Phiri and J. Morgenroth, "Developments in Landsat land cover classification methods: A review," *Remote Sens.*, vol. 9, no. 9, 2017.
- [9] M. Emimal, "Classification of Remote Sensing Images using Wavelet Based Contourlet Transform and Accuracy Analysis of Classified Images," vol. 3606, pp. 3601–3605, 2018.
- [10] L. Missions and E. Since, "Landsat — Earth Observation Satellites Landsat Missions : Imaging the Earth Since 1972," vol. 2020, no. August, pp. 2013–2016, 2016.
- [11] NASA, "Landsat 8," *Landsat Sci.*, 2017.
- [12] I. E. Issa, Doctoral ThEsis Sedimentological and Hydrological Investigation of Mosul

- Dam Reservoir Issa Elias Issa. 2011.
- [13] K. Tempfli *et al.*, “Principles of Remote Sensing.”
- [14] N. Resources, “Fundamentals of remote sensing,” *Resour. Policy*, vol. 2, no. 1, p. 65, 1976.
- [15] J. R. Eastman, “Introduction to Remote Sensing and Image Processing,” *Clark Univ. USA*, vol. 1, pp. 17–34, 2001.
- [16] M. H. Ismail, “Use of Remote Sensing and GIS in Monitoring Water Quality Use of Remote Sensing and GIS in Monitoring Water Quality,” no. August 2010, 2014.
- [17] D. Peng, “World ’ s largest Science , Technology & Medicine Open Access book publisher c,” *Agric. Biol. Sci. Grain Legum.*, 2016.
- [18] S. Koponen, *Remote sensing of water quality for Finnish lakes and coastal areas*. 2006.
- [19] J. C. Ritchie, P. V Zimba, and J. H. Everitt, “Remote Sensing Techniques to Assess Water Quality,” no. January, 2015.
- [20] S. Reis and H. M. Yilmaz, “Temporal monitoring of water level changes in Seyfe Lake,” 2008.
- [21] Bayat, O. Intersymbol interference cancellation in CDMA 1xEVDO network. *International Journal of Communication Systems*, 27(10), 2014 , P. 1553-1560.
- [22] Y. O. U. Are *et al.*, “Resolutions of Remote Sensing,” *PhD Thesis*, vol. 5, no. 2, p. 78300A, 2015.
- [23] Ucan, O. N. & Bayat, O. Performance of Face Recognition System Using Gradient Laplacian Operators and New Features Extraction. **2018**, (2018).
- [24] Biodiversity Informatics and Geospatial Innovation Facilities, “Landsat Spectral Band Information,” *Reference*, vol. 6, pp. 6–7, 2008.
- [25] S. K. McFeeters, “Using the normalized difference water index (ndwi) within a

- geographic information system to detect swimming pools for mosquito abatement: A practical approach,” *Remote Sens.*, vol. 5, no. 7, pp. 3544–3561, 2013.
- [26] H. Xu, “Modification of normalised difference water index ( NDWI ) to enhance open water features in remotely sensed imagery,” vol. 27, no. 14, pp. 3025–3033, 2006.
- [27] D. A. De Alwis, Z. Easton, H. E. Dahlke, and W. Philpot, “Unsupervised classification of saturated areas using a time series of remotely sensed images,” no. September, 2007.
- [28] W. Li *et al.*, “A comparison of land surface water mapping using the normalized difference water index from TM, ETM+ and ALI,” *Remote Sens.*, vol. 5, no. 11, pp. 5530–5549, 2013.
- [29] P. Scheunders, S. Livens, and D. Van Dyck, “Wavelet-based Texture Analysis,” no. February, 2000.
- [30] P. Arellano, “Missing information in Remote Sensing: Wavelet approach to detect and remove clouds and their shadows,” 2003.
- [31] B. U. Shankar, S. K. Meher, and A. Ghosh, “Author ’ s personal copy Wavelet-fuzzy hybridization : Feature-extraction and land-cover classification of remote sensing images.”
- [32] P. Kupidura and M. Jakubiak, “The morphological filtering of the remote sensing images for the noise reduction comparing to traditional filters,” *Ann. Geomatics*, vol. 7, no. 2 (32), pp. 63–68, 2009.
- [33] R. Frigato, “Mathematical Morphology Application To Features Extraction in Digital Images,” 2008.
- [34] M. Pesaresi and J. A. Benediktsson, “A new approach for the morphological segmentation of high-resolution satellite imagery,” *IEEE Trans. Geosci. Remote Sens.*, vol. 39, no. 2, pp. 309–320, 2001.
- [35] J. Al-doski, S. B. Mansor, H. Zulhaidi, and M. Shafri, “Image classification in remote sensing,” *J. Environ. Earth Sci.*, vol. 3, no. 10, pp. 141–148, 2013.
- [36] K. Venkateswaran, N. Kasthuri, K. Balakrishnan, and K. Prakash, “Performance Analysis

of K-Means Clustering For Remotely Sensed Images,” pp. 23–27.

- [37] B. Usman, “Satellite Imagery Land Cover Classification using K-Means Clustering Algorithm : Computer Vision for Environmental Information Extraction Satellite Imagery Land Cover Classification using K-Means Clustering Algorithm Computer Vision for Environmental Information Extraction,” no. May, 2014.
- [38] O. Ri, P. Xvlqj, and P. Ojrulwkp, “unsupervised classification of remote sensing images using K-means,” vol. 7, no. 2, pp. 548–552, 2016.
- [39] F. Roli and G. Fumera, “Support Vector Machines for Remote-Sensing Image Classification.”
- [40] M. Pal and P. M. Mather, “Support vector machines for classification in remote sensing,” no. March, 2005.
- [41] H. Elmannai, M. A. Loghmari, and M. S. Naceur, “Support Vector Machine for Remote Sensing image classification,” vol. 2, pp. 68–72, 2013.
- [42] T. Jin and R. Sensing, “High Efficient Classification On Remote Sensing Images Based,” vol. 1, no. 3, pp. 1011–1014.
- [43] C. P. Dave, “A Survey on Geometric Correction of Satellite Imagery,” vol. 116, no. 12, pp. 24–27, 2015.
- [44] U. S. G. Survey, “Landsat 8 (L8) Data Users Handbook,” *America (NY)*, vol. 8, no. 1993, pp. 1993–1993, 2005.
- [45] N. Panigrahi, B. K. Mohan, and G. Athithan, “Pre-processing algorithm for rectification of geometric distortions in Satellite images,” *Def. Sci. J.*, vol. 61, no. 2, pp. 174–179, 2011.
- [46] X. Xiao, S. Wdowinski, and Y. Wu, “Improved water classification using an application-oriented processing of landsat ETM+ and ALOS PALSAR,” *Int. J. Control Autom.*, vol. 7, no. 11, pp. 373–388, 2014.
- [47] L. Belhallouche, K. Belloulata, and K. Kpalma, “A New Approach to Region Based Image Retrieval using Shape Adaptive Discrete Wavelet Transform,” *Int. J. Image*,

- Graph. Signal Process.*, vol. 8, no. 1, pp. 1–14, 2016.
- [48] M. Matsuoka, T. Tadono, and H. Yoshioka, “Simulation of pan-sharpening using hyperspectral data to evaluate the method and band combinations,” *ACRS 2015 - 36th Asian Conf. Remote Sens. Foster. Resilient Growth Asia, Proc.*, vol. 2, pp. 2–6, 2015.
- [49] J. Schmedtmann and M. L. Campagnolo, “Reliable crop identification with satellite imagery in the context of Common Agriculture Policy subsidy control,” *Remote Sens.*, vol. 7, no. 7, pp. 9325–9346, 2015.
- [50] R. Rani and K. Kaur, “International Journal of Advanced Research in Implementation for Gabor Filter Using on Satellite Enhance the Image Quality,” *Int. J. Adv. Res. Comput. Sci. Softw. Eng.*, vol. 3, no. 5, pp. 1129–1132, 2013.
- [51] “J. Soria-Ruiz and Y. M. Fernández-Ordoñez, “Crop discrimination using remote sensing data in a region of high marginalization,” *2017 IEEE International Geoscience and Remote Sensing Symposium (IGARSS)*, Fort Worth, TX, 2017, pp. 3031-3034. doi: 10.1109/IGARSS.2017.8127637
- [52] N. Panigrahi, B. K. Mohan, and G. Athithan, “Pre-processing Algorithm for Rectification of Geometric Distortions in Satellite Images,” vol. 61, no. 2, pp. 174–179, 2011.
- [53] R. Mishra, “Contrast Enhancement of Remote Sensing Images using DWT with Kernel Filter and DTCWT,” vol. 87, no. 17, pp. 43–49, 2014.
- [54] H. Jiang, M. Feng, Y. Zhu, N. Lu, J. Huang, and T. Xiao, “An automated method for extracting rivers and lakes from Landsat imagery,” *Remote Sens.*, vol. 6, no. 6, pp. 5067–5089, 2014.
- [55] J. Mcgee, J. Campbell, and T. Parece, “Remote Sensing in an ArcMap Environment,” *Remote Sens. an ArcMap Environ.*, 2014.
- [56] S. Ahmed Medjahed, “A Comparative Study of Feature Extraction Methods in Images Classification,” *Int. J. Image, Graph. Signal Process.*, vol. 7, no. 3, pp. 16–23, 2015.
- [57] G. Sarp and M. Ozcelik, “Water body extraction and change detection using time series :

- A case study of Lake Burdur , Turkey,” *Integr. Med. Res.*, vol. 11, no. 3, pp. 381–391, 2017.
- [58] K. Rokni, A. Ahmad, A. Selamat, and S. Hazini, “Water feature extraction and change detection using multitemporal landsat imagery,” *Remote Sens.*, vol. 6, no. 5, pp. 4173–4189, 2014.
- [59] L. Resource, U. S. E. Patterns, A. In, U. Satellite, and R. Sensing, “International Journal of Remote Simultaneous detection of burned areas of multiple fires in the tropics using multisensor remote-sensing data,” no. July 2012, 2017.
- [60] K. Parvathi, B. S. P. Rao, and T. V. Rao, “International Journal of Remote Feature extraction from satellite images of hilly terrains using wavelets and watersheds,” *Int. J. Remote Sens.*, vol. 1161, no. March 2012, pp. 37–41, 2010.
- [61] J. Daryaei, “Digital change detection using multi-scale wavelet transformation & neural network,” *Int. Inst. Aerosp. Surv. ...*, no. January, 2003.
- [62] L. Belhallouche, “A New Approach to Region Based Image Retrieval using Shape Adaptive Discrete Wavelet Transform,” no. January, pp. 1–14, 2016.
- [63] R. Frigato, “Mathematical Morphology Application to Features Extraction in Digital Images,” 2008.
- [64] K. Yang, M. Li, Y. Liu, L. Cheng, Q. Huang, and Y. Chen, “River detection in remotely sensed imagery using Gabor filtering and path opening,” *Remote Sens.*, vol. 7, no. 7, pp. 8779–8802, 2015.
- [65] H. K. Singh, “Thresholding Techniques applied for Segmentation of RGB and multispectral images,” no. June, 2016.
- [66] B. S. Morse, “Lecture 4: Thresholding,” *Reading*, pp. 1998–2000, 2000.
- [67] M. Jakubiak, “The Morphological Filtering of the remote sensing images for the noise reduction comparing to traditional filters Non-morphological filters Basics of mathematical morphology and morphological filtering,” 2009.

- [68] Abhishek R and Srinivas N, "An Advanced Technique for Removal Of Salt & Pepper Noise In Images," *Int. J. Eng. Comput. Sci.*, vol. 2, no. 2, pp. 2319–7242, 2013.
- [69] F. R. Project, "A Review of Assessing the Accuracy of and of Methods Including Remote Sensing Data in Forest Inventory," no. November, 1998.
- [70] Abu baker Haroun Mohamed Adam , and etl." Accuracy Assessment of Land Use & Land Cover Classification (LU/LC) "Case study of Shomadi areaRenk County-Upper Nile State, South Sudan", *International Journal of Scientific and Research Publications*, Volume 3, Issue 5, May 2013 1 ISSN 2250-3153
- [71] P. Chaudhary, S. Godara, A. N. Cheeran, and A. K. Chaudhari, "Fast and Accurate Method for Leaf Area Measurement," vol. 49, no. 9, pp. 22–25, 2012.
- [72] R. K. Nath and S. K. Deb, "Water-Body Area Extraction From High Resolution Satellite Images-An Introduction, Review, and Comparison," *Int. J. Image Process.*, vol. 3, no. 3, pp. 353–372, 2010.
- [73] I. E. Issa and N. Al-ansari, "Changes in Bed Morphology of Mosul Dam Reservoir," *J. Adv. Sci. Eng. Res.*, vol. 3, no. 2, pp. 86–95, 2013.
- [74] Y. Liu, X. Wang, F. Ling, S. Xu, and C. Wang, "Analysis of Coastline Extraction from Landsat-8 OLI Imagery," pp. 1–26, 2017.
- [75] L. Ji, X. Geng, K. Sun, Y. Zhao, and P. Gong, "Target Detection Method for Water Mapping Using Landsat 8 OLI/TIRS Imagery," *Water*, vol. 7, no. 2, pp. 794–817, 2015.
- [76] G. Shaw and H. Burke, "Spectral Imaging for Remote sensing," *Lincoln Lab. J.*, vol. 14, no. 1, pp. 3–28, 2003.
- [77] G. Kaplan and U. Avdan, "Object-based water body extraction model using Sentinel-2 satellite imagery," *Eur. J. Remote Sens.*, vol. 50, no. 1, 2017.
- [78] O. O. Omo-Irabor and K. Oduyemi, "A hybrid image classification approach for the systematic analysis of land cover (LC) changes in the Niger Delta region," *Proc. 15th Int. Symp. Spat. Data Qual. Enschede, Netherlands*, no. LC, p. 7, 2007.



- [79] S. D. Jawak, K. Kulkarni, and A. J. Luis, "A Review on Extraction of Lakes from Remotely Sensed Optical Satellite Data with a Special Focus on Cryospheric Lakes," *J*, vol. 4, no. 4, pp. 196–213, 2015.
- [80] K. Radhika, "A tutorial on classification of remote sensing data 1," pp. 881–885, 2016.
- [81] A. Description, "K-means Algorithm g," pp. 1–16, 2012.
- [82] F Sardouk, AD Duru, O Bayat . Classification of Breast Cancer Using Data Mining, *American Scientific Research Journal for Engineering*, 51(1), P.38-46, 2019.
- [83] P.-N. Tan, M. Steinbach, and V. Kumar, "Chap 8 : Cluster Analysis: Basic Concepts and Algorithms," *Introd. to Data Min.*, p. Chapter 8, 2005.
- [84] "Accuracy Assessment of the Discrete Classification of Remotely-Sensed Digital Data for Landcover Mapping by," 1995.
- [85] L. Cai, "Accuracy Assessment Measures for Object Extraction from Remote Sensing Images."
- [86] R. Zaki, A. Zaki, and S. Ahmed, "Land Use and Land Cover Changes in Arid Region: The Case New Urbanized Zone, Northeast Cairo, Egypt," *J. Geogr. Inf. Syst.*, vol. 03, no. 03, pp. 173–194, 2011.
- [87] 1 Shravan Kumar Yadav, 2 Shubhangi Raj, 3 Shyam Sundar Roy, Remote Sensing Technology And Its Applications. *International Journal of Advancements in Research & Technology*, Volume 2, Issue 10, October-2013 25 ISSN 2278-7763, P.25-30.
- [88] I. E. Issa and N. Al-ansari, "Changes in Bed Morphology of Mosul Dam Reservoir," *Journal of Advanced Science and Engineering Research*, vol. 3, no. 2. pp. 86–95, 2013.
- [89] L. Bolelli, S. Ertekin, D. Zhou, and C. L. Giles, "K-SVMMeans : A Hybrid Clustering Algorithm for Multi-Type Interrelated Datasets," pp. 198–204, 2007.
- [90] R. P. Gupta, R. K. Tiwari, V. Saini, and N. Srivastava, "A Simplified Approach for Interpreting Principal Component Images," *Adv. Remote Sens.*, vol. 02, no. 02, pp. 111–119, 2013.

- [91] P. Yousefi, H. A. Jalab, R. W. Ibrahim, N. F. M. Noor, M. N. Ayub, and A. Gani, "Water-Body Segmentation in Satellite Imagery Applying Modified Kernel K-Means. pp. 143-154," vol. 31, no. 2, pp. 143–154, 2018.
- [92] L. Use, "Analysis And Comparative study of Image Fusion Techniques For Landuse Landcover Classification/Chapter 5," in *Analysis And Comparative study of Image Fusion Techniques For Landuse Landcover Classification*, .
- [93] C. Ding, "K -means Clustering via Principal Component Analysis," 2004.
- [94] C. Lagoon, "PCA Classification Technique of Remote Sensing Analysis of Colour Composite International Journal of Advanced Research in PCA Classification Technique of Remote Sensing Analysis of Colour Composite Image of Chillika Lagoon , Odisha," no. July 2015, 2013.
- [95] D. S. S. Baboo and M. R. Devi, "An Analysis of Different Resampling Methods in Coimbatore, District," *Glob. J. Comput. Sci. Technol.*, vol. 10, no. 15, pp. 61–66, 2010.
- [96] G. Palubinskas, "Fast, simple, and good pan-sharpening method," *J. Appl. Remote Sens.*, vol. 7, no. 1, p. 073526, 2013.
- [97] B. Johnson, R. Tateishi, and N. Hoan, "Satellite Image Pansharpening Using a Hybrid Approach for Object-Based Image Analysis," *ISPRS Int. J. Geo-Information*, vol. 1, no. 3, pp. 228–241, 2012.
- [98] O. Dalmau, T. Alarcón, and F. Oliva, "Crop Classification in Satellite Images through Probabilistic Segmentation Based on Multiple Sources," *Sensors*, vol. 17, no. 6, p. 1373, 2017.
- [99] R. Bekkerman and A. McCallum, "Multi-Way Distributional Clustering via Pairwise Interactions," 2005.
- [100] V. Sourirajan, "A TUTORIAL ON CLASSIFICATION OF REMOTE SENSING DATA," no. August, 2018.

- [101] A. Shrivastava and R. R. Ahirwal, "A SVM and K-means Clustering based Fast and Efficient Intrusion Detection System," vol. 72, no. 6, pp. 25–29, 2013.
- [102] M. Perumal and M. Jayaprakash, "Landuse / Landcover Change Detection Analysis Using and Remote Sensing -in and Around Manakudy Estuary , SW Coast Of India," no. July, 2014.
- [103] F. A. Vertuccil, "Spectral reflectance and water quality of Adirondack mountain region lakes," vol. 34, no. 8, pp. 1656–1672, 1989.
- [104] O.Bayat, B.Shafai, and et al, "Signalling enhancement on multilevel turbo codes," *Int. J. Common. Syst.* 2008; 21:791–798, published online 25 February 2008 in Wiley InterScience ([www.interscience.wiley.com](http://www.interscience.wiley.com)). DOI: 10.1002/dac.928.
- [105] Mustafa and Bayat , " Water surface area detection using remote sensing temporal data processed using MATLAB", *International Journal of Electrical Engineering& Education(IJEEE)*,2019,PP.1-13,[sagepub.com/journals-permissions](http://sagepub.com/journals-permissions) DOI:10.1177/0020720919851500 , [journals.sagepub.com/home/ije](http://journals.sagepub.com/home/ije).